# Atmospheric parameters and chemical abundances of the A-type eclipsing binary system RR Lyncis A and B

Yoichi Takeda<sup>1</sup>

<sup>1</sup>11-2 Enomachi, Naka-ku, Hiroshima-shi, 730-0851, Japan \*Corresponding author. E-mail: ytakeda@js2.so-net.ne.jp

MS received; accepted

Abstract. A spectroscopic study was carried out for the double-line A-type eclipsing binary system RR Lyn A+B based on the disentangled spectra, with an aim of clarifying the differences in photospheric chemical compositions between the components, where  $T_{\rm eff}$  (effective temperature) and  $v_{\rm t}$  (microturbulence) were determined from Fe lines. The resulting abundances of 30 elements revealed the following characteristics. (1) The brighter/hotter A shows metal-rich trends of classical Am stars; i.e., heavier elements generally show overabundances tending to increase towards higher Z (atomic number) with exceptionally large deficit of Sc, while light elements such as CNO show underabundances. (2) Meanwhile, the abundances of fainter/cooler B are closer to the solar composition ([X/H]  $\sim$  0 for intermediate Z elements such as Fe group) though [X/H] does exhibit a slightly increasing tendency with Z, which suggests that B is a kind of marginal Am star with almost normal metallicity. This consequence is in contrast to the results of previous studies, which reported B to be of metal-deficient nature similar to  $\lambda$  Boo stars. Such distinctions of chemical abundances between A and B may serve as a key to understanding the condition for the emergence of Am phenomenon.

**Keywords.** stars: abundances — stars: atmospheres — stars: binaries: spectroscopic — stars: chemically peculiar — stars: early-type — stars: individual (RR Lyn)

## 1. Introduction

It is a long-standing problem which has been attracted stellar spectroscopists that a fraction of A- and late B-type stars on the upper main sequence show various kinds of compositional anomalies. Although the basic classification scheme of these chemically peculiar stars of diversified characteristics (e.g., Si stars, SrCrEu stars, Am stars, HgMn stars,  $\lambda$  Boo stars, etc.) was almost established about a half century ago (e.g., Preston 1974), our understanding on the nature and origin of their chemical anomalies is still far from satisfactory.

One of the key approaches to clarify the condition for the emergence of chemical peculiarities is to study and compare the abundances of the components of double-line spectroscopic binaries, because both should have had the same compositions when they were born. In particular, eclipsing binaries would be preferable, since their stellar parameters are more precisely determinable. Yet, chemical abundance determinations of double-line binaries generally suffer considerable difficulties, because spectral lines are so intricately mixed that reliable measurements of line strengths for both components on the composite spectra are not easy to practice.

Fortunately, the advent of the efficient spectrumdisentangling technique, which can numerically reproduce the spectra of both components as resolved (thanks to the improved computational power and availability of high-S/N and high-resolution spectra nowadays), changed this situation dramatically.

Takeda et al. (2019; hereinafter referred to as Paper I) applied this method to the spectra of five eclipsing binaries (AR Aur,  $\beta$  Aur, WW Aur, YZ Cas, and RR Lyn) covering various phases to obtain the disentangled spectra in five selected regions. Then, the chemical abundances of several elements (with the main attention being paid to light elements such as CNO) were determined for both components in order to discuss the compositional differences between them.

Especially important is a system of two stars with rather similar parameters, where one shows a distinct type of chemical peculiarity while the other does not. AR Aur corresponds to such an interesting case; i.e., the primary (A) is a typical HgMn star but such an anomaly is not seen in the secondary (B), despite that both are similar late B-type stars. Accordingly, the author recently carried out an extensive reanalysis of this binary system by fully exploiting the disentangled spectra of wide wavelength ranges (Takeda 2025;

hereinafter Paper II), where the stellar parameters [ $T_{\rm eff}$  (effective temperature) and  $v_{\rm t}$  (microturbulence)] were spectroscopically determined from many Fe lines and the abundances of 28 elements were derived (the non-LTE effect was taken into account for 10 elements). The typical characteristics of HgMn peculiarities with large dispersion (very deficient N, Al, Sc, Ni or very overabundant P, Mn) were then confirmed in A, while B was found to show a comparatively weak and rather organized peculiarity (almost linearly increasing with the atomic number Z). It is interesting that such remarkably dissimilar types of chemical peculiarities are observed in A and B (with only a small  $T_{\rm eff}$  difference of  $\sim 500$  K).

RR Lyn is also counted as such an interesting eclipsing binary system (orbital period is  $P=9.95\,\mathrm{d}$ ) consisting of two late A-type stars ( $T_\mathrm{eff}$  differs by at least several hundred K), where the brighter A is a Am star of metal-rich character while the chemical composition of the fainter B is distinctly different (reported to be even metal-poor). Therefore, it is worthwhile to investigate the differences of physical properties (in terms of stellar parameters and chemical abundances) between RR Lyn A and B as precisely as possible, which may provide us with a key to understanding the condition for the advent of Am phenomenon.

Unfortunately, despite that not a few investigators carried out spectroscopic studies on this binary system as briefly summarized in Table 1, the results reported in these previous publications are diversified and unconformable, from which the problematic points may be identified as follows.

- Since the luminosity of B is appreciably lower (~ 25–30%) than that of A, line strengths of B appear much weaker than those of A due to the dilution effect, which means that measuring B's spectral lines in the composite spectra is a difficult task. Actually, studies of RR Lyn in the old days based on data of low-quality photographic spectrograms had to regard RR Lyn A+B as if a single star (~ A), disregarding the lines of B. Most of the other investigations laboriously measured the lines of A and B separately in the A+B mixed spectra, though the number of available lines was comparatively limited in this approach. It is only the analysis of Paper I that employed disentangled spectra for this star.
- Thanks to the merit of eclipsing binary,  $\log g$  (surface gravity) values for A and B are precisely determined in this system. However,  $T_{\rm eff}$  and  $v_{\rm t}$  values adopted in previous studies, which play significant roles in abundance determinations, are considerably diversified ( $T_{\rm eff}$  differ-

- ences amounting to  $\lesssim 600-700$  K and  $v_t$  being discrepant by  $\lesssim 50-100\%$ ) as can be recognized in Table 1. These parameters have to be more reliably established by all means; most preferably by the spectroscopic method using many lines.
- Almost all previous investigations concluded that the brighter A is metal-rich (though its extent appreciably differs from each other), which is reasonably understandable because A is believed to be a typical Am star. Meanwhile, it is rather puzzling that the fainter B was reported to be mildly metal-poor ([Fe/H] is  $\sim -0.2$  to  $\sim -0.4$ ) in most of the past studies. Such a subsolar metallicity is hard to understand for a comparatively young population I star. Admittedly, there is a group of chemically peculiar stars (so-called  $\lambda$  Boo stars) which show deficiencies in refractory Fe group elements (presumably caused by dust-gas separation mechanism) while volatile elements (such as CNO) remain almost normal (see, e.g., Venn & Lambert 1990). Actually, Jeong et al. (2017) affirmed that RR Lyn B is a  $\lambda$  Boo star. It should be noted, however, that  $\lambda$  Boo stars are generally known to be rapid rotators. Since both RR Lyn A and B are evidently slow rotators, this argument needs to be viewed with caution. It is thus of primary importance to check (by precise determinations of [Fe/H] based on many lines) whether or not B is really underabundant in metals.

These problems motivated the author to carry out a new spectroscopic study on the RR Lyn A+B system in a similar manner to that adopted for AR Aur (Paper II), which is a refined and extended analysis (compared to that of Paper I) where the main attention is paid to the following points.

- Disentangled spectra are obtained for as wide wavelength regions as possible (from violet to near infrared), which makes measurements of equivalent widths for a large number of spectral lines (~ 1000) feasible.
- In contrast to Paper I, where catalogue values were assigned to  $T_{\rm eff}$  (which are originally the photometric determinations of Khaliullin e al. 2001) and Takeda et al.'s (2008) empirical  $T_{\rm eff}$ -dependent formula was employed for  $v_{\rm t}$ , ( $T_{\rm eff}$ ,  $v_{\rm t}$ ) are spectroscopically established from a number of Fe lines by requiring the consistency of abundances (as done in Paper II).
- Based on such determined atmospheric parameters, chemical abundances of many elements

are derived (mainly from the measured equivalent width or additionally by using the spectrumfitting technique), where the non-LTE is taken into account wherever possible (as in Paper II).

## 2. Observational Data

## 2.1 Spectrum disentangling

The basic observational materials are the high-dispersion spectra of RR Lyn (resolving power is  $R \simeq 45000$ ) covering wide wavelength ranges ( $\sim 3800-9200$  Å), which were obtained on 2010 December 14, 15, 16, 18, and 20 by using BOES (Bohyunsan Observatory Echelle Spectrograph) attached to the 1.8 m reflector at Bohyunsan Optical Astronomy Observatory (cf. Sect. 2.1 and Table 2 of Paper I for more details of these data).

Then, the separated spectra of A and B were numerically obtained by applying the spectrum-disentangling technique to a set of nine double-line (A+B) spectra at 9 different phases, where the public-open software CRES<sup>2</sup> written by Dr. S. Ilijić was employed with the same procedure as detailed in Sect. 2.2 of Paper I.

Likewise, the same preconditioning processes as done in Paper II were applied beforehand to the original spectra: (1) Continuum normalizations of all original spectra were done by regarding the wings of very strong lines (e.g., H lines) as if being the pseudo-continuum level, so that these features may be eventually wiped out in the final spectra. (2) Telluric features were removed in advance by dividing the spectrum by that of a rapid rotator or by erasing them interactively by hand on the screen.

In consequence, disentangled spectra of RR Lyn A and B in 69 spectral regions (segments of typically several tens Å to  $\sim 100$  Å wide; partially overlapped with each other) were obtained, which cover from  $\sim 3900$  Å to  $\sim 9200$  Å with a step of  $\sim 0.05$  Å. The overall trends of these spectra are displayed in Fig. 1a (A) and 1b (B), and how the signal-to-noise ratio depend upon the wavelength is also shown in Fig. 1c (A) and 1d (B). We can see that (i) S/N for A ( $\lesssim 500$ –800) is appreciably higher than that for B ( $\lesssim 200$ ) and (ii) the maximum S/N is attained around  $\sim 6000$  Å. All these spectra used for the analysis are included in the online materials ("specdata\_A.txt" and "specdata\_B.txt").

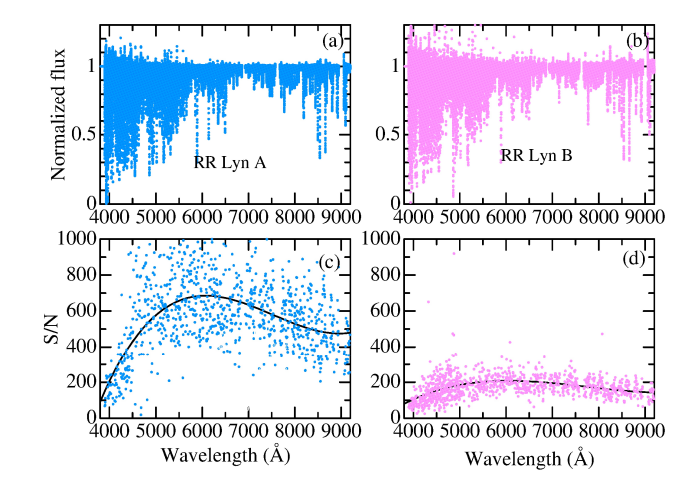


**Figure 1**. The whole disentangled spectra of RR Lyn A and B used in this study are plotted against wavelength in the upper panels (a) and (b). The runs of signal-to-noise ratios of these spectra (directly estimated in line-free regions) are shown in the lower panels (c) and (d), where the fitted 3rd-order polynomials (describing the global trends) are also depicted by solid lines.

## 2.2 Line identification and equivalent widths

Based on the disentangled spectra, lines usable for abundance determinations were identified and their equivalent widths were measured. The identification was done by carefully comparing the observed and theoretically synthesized spectra with each other. Here, lines to be measured were restricted to only those of single component (i.e., multiplet lines with fine structures such as Mg II 4481 were discarded), and those being seriously affected by blending with other neighborhood lines were avoided.

The equivalent width  $(W_{\lambda})$  of each line was evaluated by applying the Gaussian fitting to its profile. Fig. 2 demonstrates how the equivalent widths were actually measured for selected 24 lines of different element species. All the data  $(W_{\lambda}$  along with the atomic data taken from the VALD database; cf. Ryabchikova et al. 2015) of finally identified 1364/1382 lines for A/B are also presented as the online material ("ewlines\_A.txt" and "ewlines\_B.txt").

<sup>&</sup>lt;sup>1</sup>The first spectrum on Dec. 14 coded "rrlyn\_20101214A" (cf. Table 2 in Paper I) was not used because it corresponds to the eclipse phase.

<sup>&</sup>lt;sup>2</sup>http://sail.zpf.fer.hr/cres/

Authors	$T_{\rm eff,A}$	$\log g_{\rm A}$	$v_{\mathrm{t,A}}$	[Fe/H] <sub>A</sub>	$T_{\rm eff,B} \log g_{\rm B}$	$v_{t,B}$	[Fe/H] <sub>B</sub>
	(K)		$(km s^{-1})$	(dex)	,	$(km s^{-1})$	(dex)
Smith (1971)	(8125)		(7.0)	(6.74)*			
Rachkovskaya (1974)	$(7750)^{\#}$		(4.7)				
Kondo (1976)	8100	3.91	7.0	7.32*	6900 4.07	3.0	6.54*
Burkhart & Coupry (1991)	7960			+0.35	7500		-0.3
Lyubimkov & Rachkovskaya (1995b)	(7850)	(3.95)	(5.8)	(+0.11)			
Lyubimkov & Rachkovskaya (1995a,b)	8020	3.91	6.3	+0.27	7150 4.07	2.1	-0.33
Kunzli & North (1998)	(7581)	(3.76)	(3.2)	$(+0.15)^{\dagger}$			
Hui-Bon-Hoa (2000)	8240	4.00	3.0	+0.66	7610 4.10	2.5	-0.19
Khaliullin et al. (2001)	7570	3.89		$+0.31^{\dagger}$	6980 4.21		$-0.24^{\dagger}$
Jeong et al. (2017)	7920	3.80	4.6	+0.20	7210 4.16	3.2	-0.34
Takeda et al. (2019) (Paper I)	7570	3.90	3.8	+0.11	6980 4.21	3.1	-0.41
This study	7990	3.90	3.5	+0.37	7570 4.20	2.6	-0.01

**Table 1.** Stellar parameters of RR Lyn A and B adopted in previous investigations.

The  $T_{\rm eff}$  (in K),  $\log g$  (in dex; g is in unit of cm s<sup>-2</sup>),  $v_{\rm t}$  (in km s<sup>-1</sup>) and [Fe/H] (Fe abundance relative to the Sun; in dex) adopted in the past literature are given in column 2–5 (RR Lyn A) and column 6–9 (RR Lyn B). The parenthesized values for old studies (Smith 1971; Rachkovskaya 1974; Lyubimkov & Rachkovskaya 1995b; Kunzli & North 1998) are those derived by regarding RR Lyn as if a single star, which may be regarded as almost corresponding to the brighter A. Regarding the projected rotational velocity ( $v_{\rm e} \sin i$ ), Takeda et al. (2019) derived 15.2 km s<sup>-1</sup> (A) and 11.6 km s<sup>-1</sup> (B) based on the spectrum-fitting analysis applied to the O I 7771–5 feature.

Metallicity [M/H] derived from colors.

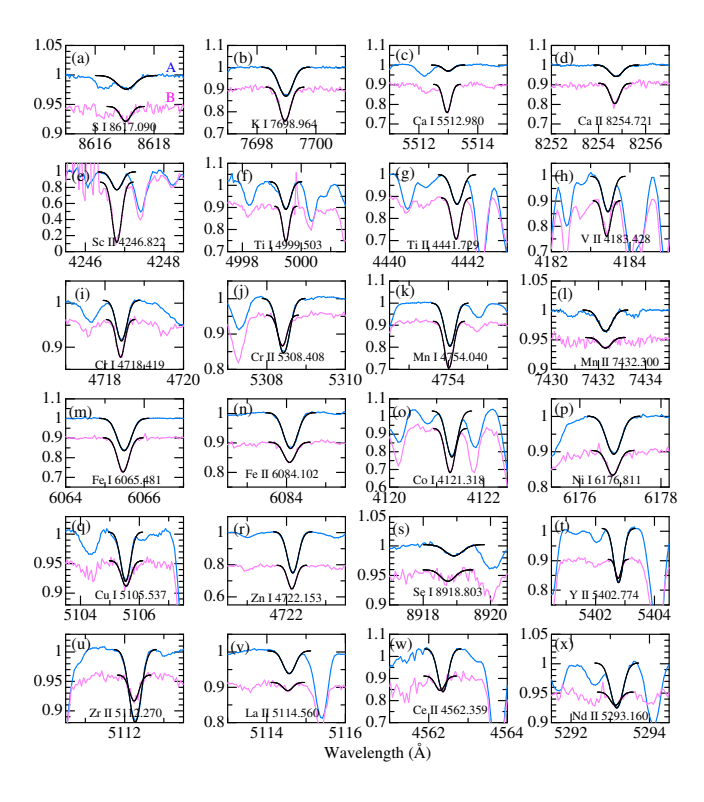


**Figure 2**. In order to demonstrate how the equivalent widths were measured by the Gaussian fitting, selected cases of 24 lines (as indicated in each panel) are shown here. The observed spectra are drawn in color (blue for A, pink for B), while the fitted curve is depicted by a black line. The scale in the ordinate is for A, since the spectra for B are shifted downwards by appropriate amounts (0.05 or 0.1 or 0.2).

## 3. Atmospheric Parameters

## 3.1 Basic principles

One of the objectives of this study is to establish  $T_{\rm eff}$ and  $v_t$  for both RR Lyn A and B by making use of many Fe lines, as done in Paper II. As well known,  $T_{\rm eff}$  can be determined by the requirement that the abundances  $(A_i)$  derived from the equivalent widths  $(W_i)$  of each line i (i = 1, 2, ..., N; where N is the number of lines) do not systematically depend upon the lower excitation potential  $(\chi_{low})$  [excitation equilibrium], while  $v_t$  is determinable by demanding that  $A_i$ 's do not show any systematic trend irrespective of the equivalent widths  $(W_i)$ or reduced equivalent widths ( $\equiv 10^6 W_i/\lambda_i$ ) [curve-ofgrowth matching]. The desired solution  $(T_{eff}^*, v_t^*)$  simultaneously satisfying these two conditions can be obtained by finding the minimum of  $\sigma(T_{\text{eff}}, v_t)$ , where  $\sigma$  is the standard deviation of the abundances around the mean  $(\langle A \rangle)$  calculated for various combinations of  $(T_{\rm eff}, \nu_{\rm t}).$ 

## 3.2 Line selection

In the first place, some preparatory analysis may be in order, in order to define the set of lines to be used for the analysis by rejecting unsuitable lines. For this purpose, Fe abundances (A) were calculated from the  $W_{\lambda}$  values of all Fe lines measured in Sect. 2.2 by using the ( $T_{\rm eff}$ ,  $\log g$ ,  $v_{\rm t}$ ) values adopted in Paper I [(7570,

<sup>\*</sup>Excitation temperature determined from Fe I lines.

<sup>\*</sup>Absolute abundance (in the usual normalization of H = 12) is given here, because the solar Fe abundance relevant to such an old analysis (based on unreliable gf values as viewed from the present-day standard) is difficult to assign.

3.90, 3.8) for A and (6980, 4.21, 3.1) for B] as the starting trial parameters. The resulting A values are plotted against  $10^6 W_{\lambda}/\lambda$  and  $\chi_{\text{low}}$  in Fig. 3. An inspection of Fig. 3a,b (A) and Fig. 3e,f (B) shows that a rather abrupt upturn of A is seen at  $\log(10^6 W_{\lambda}/\lambda) \gtrsim$ 0.5. Although the cause of this phenomenon is not clear (depth-dependence of  $v_t$ ?), it is certain that  $W_{\lambda}$ independence of A can not be accomplished as long as these stronger lines are included. Therefore, lines satisfying the condition  $10^6 W_{\lambda}/\lambda > 30$  (corresponding to  $W_{\lambda} > 150 \text{ mÅ}$  at  $\lambda = 5000 \text{Å}$ ) were discarded from the outset. Besides, outlier lines showing appreciable deviations were removed. The plots corresponding to those rejected lines are highlighted in light-green in Fig. 3. After the elimination process, the numbers of Fe I and Fe II lines  $(N_1, N_2)$  to be employed for the analysis in Sect. 3.3 are (522, 131) for A and (604, 78) for B.

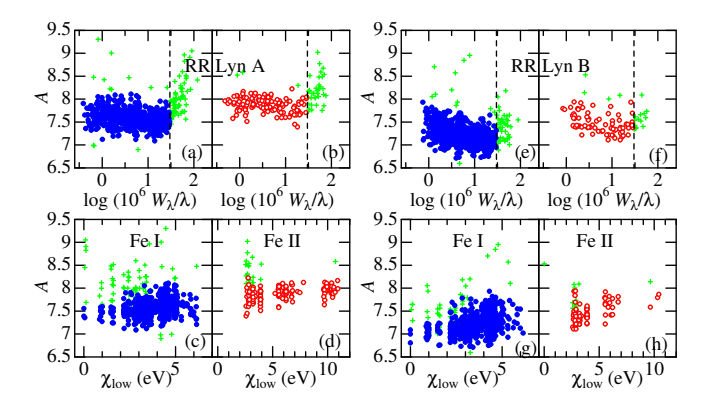


**Figure 3.** Results of the preparatory analysis for selecting suitable Fe lines to be used for spectroscopic ( $T_{\rm eff}$ ,  $v_{\rm t}$ ) determination. Plotted against  $10^6 W_{\lambda}/\lambda$  (reduced equivalent width) and  $\chi_{\rm low}$  (lower excitation potential) are the Fe abundances (A) derived from the Fe I and Fe II lines with the ( $T_{\rm eff}$ ,  $v_{\rm t}$ ) values adopted in Paper I [(7570 K, 3.8 km s<sup>-1</sup>) for A and (6980 K, 3.1 km s<sup>-1</sup>) for B]. The data corresponding to the finally adopted lines are depicted in blue filled circles (Fe I) and red open circles (Fe II), while those for the rejected lines (lines showing outlier abundances or strong lines of  $10^6 W_{\lambda}/\lambda > 30$  (this critical limit is indicated by vertical dashed lines in the relevant panels) are highlighted in lightgreen crosses. The four panels (a)–(d) on the left-hand side are for A and those of (e)–(h) on the right-hand side are for B.

# 3.3 *Solutions of* $T_{\text{eff}}$ *and* $v_{\text{t}}$

We are now ready to carry out an optimization analysis to obtain the desired solutions of  $(T_{\rm eff}, v_{\rm t})$ . For each species (Fe I or Fe II) and each star (A or B), Fe abundances  $(A_i, i = 1, 2, \dots, N)$  were calculated from the equivalent widths  $(W_i, i = 1, 2, \dots, N)$  for an extensive grid of 1066 (=41×26) cases resulting from combinations of 41  $T_{\rm eff}$  (from 6500 to 8500 K with a step

of 50 K) and 26  $v_t$  (from 1.0 to 6.0 km s<sup>-1</sup> with a step of 0.2 km <sup>-1</sup>), where the necessary model atmospheres (solar metallicity models with  $\log g = 3.9$  and  $\log g = 4.2$  for A and B; cf. Sect. 3.4) were generated by interpolating Kurucz's (1993) grid of ATLAS9 models. Then,  $\langle A \rangle$  and  $\sigma$  are calculated from the resulting set of  $(A_i, i = 1, 2, \dots, N)$  for each of the 1066 combinations of  $(T_{\text{eff}}, v_t)$ , while a few outlier data (judged by Chauvenet's criterion) were discarded in this process.

The contour maps of such obtained  $\sigma_{1A}$ ,  $\sigma_{2A}$ ,  $\sigma_{1B}$ , and  $\sigma_{2B}$  on the  $T_{\text{eff}}$ – $v_{t}$  plane are depicted in Fig. 4a, 4b, 4c, and 4d, respectively. The solutions of  $(T_{\text{eff}}^{*}, v_{t}^{*})$  at the minimum of  $\sigma$  (denoted by crosses in Fig. 4) for each case are summarized in Table 2.

The resulting  $(T_{\rm eff}^*/v_{\rm t}^*/\langle A \rangle)$  derived from Fe I and Fe II lines are read from Table 2 as  $(7990/3.5/7.85)_{\rm 1A}$  and  $(7920/4.0/7.88)_{\rm 2A}$  for A, while  $(7570/2.6/7.54)_{\rm 1B}$  and  $(7940/3.2/7.48)_{\rm 2B}$  for B, where the values are appropriately rounded.

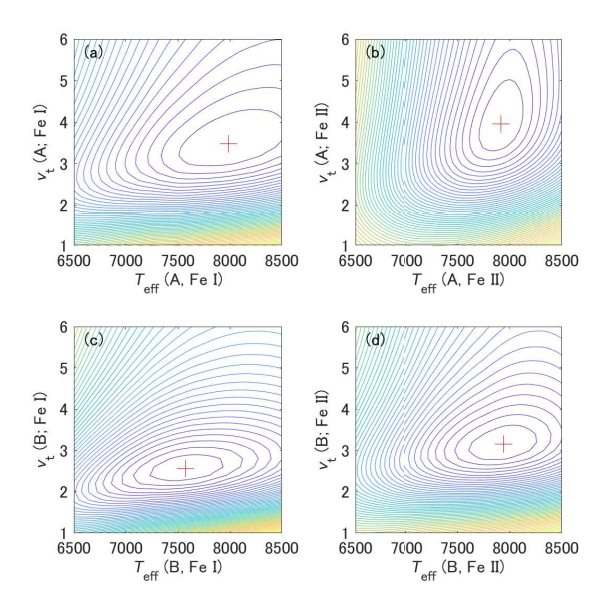


**Figure 4.** Graphical display of the contours of  $\sigma(T_{\rm eff}, \nu_{\rm t})$ , where the position of  $(T_{\rm eff}^*, \nu_{\rm t}^*)$  corresponding the minimum of  $\sigma$  is indicated by a cross. The upper panels (a, b) are for RR Lyn A, while the lower ones (c, d) are for RR Lyn B. The left panels (a, c) and the right ones (b, d) are for Fe I and Fe II, respectively.

## 3.4 Adopted parameters

Two kinds of  $(T_{\rm eff}^*, \nu_{\rm t}^*)$  solutions were derived in Section 3.3 from Fe I and Fe II lines. The next task is to decide which of these two solutions we should adopt, since both are appreciably discrepant in some cases (e.g.,  $T_{\rm eff}$  for the case of B).

In contrast to the case of AR Aur in Paper II (where the results from Fe II were eventually adopted), we consider that the solutions derived from Fe I lines are more reliable than those from Fe II lines for the present case of RR Lyn. This is because the number of Fe II lines is distinctly smaller in comparison with Fe I lines (especially for B, where  $N_2$  is only  $\sim 1/8N_1$ ) and the scatter of  $A_2$  is apparently too large to yield a convincing result as can be seen in Fig. 3f and 3h. Accordingly, the  $(T_{\text{eff}}^*, v_1^*)$  results derived from Fe I lines are adopted; i.e., (7990, 3.5) for A, and (7570, 2.6) for B.

The values of surface gravity are precisely determined for this eclipsing binary system; for example, Khaliullin e al. (2001) derived  $3.894(\pm0.019)$  (A) and  $4.214(\pm0.025)$  (B). Accordingly,  $\log g = 3.90$  (A) and 4.20 (B) are adopted in this study (essentially the same as in Paper I) with an uncertainty of  $\leq 0.05$  dex, which is practically sufficient because abundances are less sensitive to this parameter. As to the model metallicity, solar composition models are adopted (as done in Paper I and Paper II), which is sufficient because atmospheric structures of early-type stars do not depend much upon the metallicity.

The final parameters of RR Lyn A and B used for abundance determinations are summarized in Table 3, where probable uncertainties are also given. The Fe abundances ( $A_i$ ) derived from each of Fe I and Fe II lines corresponding to the adopted Fe I-based  $T_{\rm eff}^*/v_{\rm t}^*$  solutions are plotted against ( $10^6W_i/\lambda_i$ ) and  $\chi_{\rm low}$  and the relevant empirical curves of growth are depicted in the left (Fe I) and center (Fe II) columns of Fig. 5 (A) and Fig. 6 (B), where the Fe II results for the (unadopted) Fe II-based parameters are also shown in the right columns for comparison. It can be seen from these figures that the required condition (no systematic dependence in  $A_i$  upon  $W_i$  and  $\chi_{\rm low}$ ) is almost satisfied.

**Table 2.**  $(T_{\rm eff}, v_{\rm t})$  solutions at the minimum of  $\sigma$ .

Lines	$T_{ m eff}^*$	$v_{\mathrm{t}}^{*}$	$\sigma^*$	$\langle A \rangle$	Fig.				
	(K)	$(km s^{-1})$	(dex)	(dex)					
	[RR Lyn A]								
Fe 1	7989	3.48	0.177	7.851	4a				
	(175)	(0.26)							
Fe п	7916	3.96	0.128	7.881	4b				
	(94)	(0.38)							
[RR Lyn B]									
Fe 1	7575	2.56	0.193	7.537	4c				
	(199)	(0.16)							
Fe п	7943	3.15	0.142	7.475	4d				
	(182)	(0.26)		6					

Columns 2 and 3 give the values of  $T_{\rm eff}$  and  $v_{\rm t}$ , at which Fe abundance dispersion is minimized. The corresponding  $\sigma$  and the mean Fe abundance are presented in columns 4 and 5, respectively. See the figures indicated in column 6 for the relevant  $\sigma(T_{\rm eff}, v_{\rm t})$  contours. The parenthesized values are the probable uncertainties involved in  $T_{\rm eff}^*$  and  $v_{\rm t}^*$ , which were estimated from  $\sigma^*$  by random simulations as described in Sect. 3.3 of Takeda (2024).

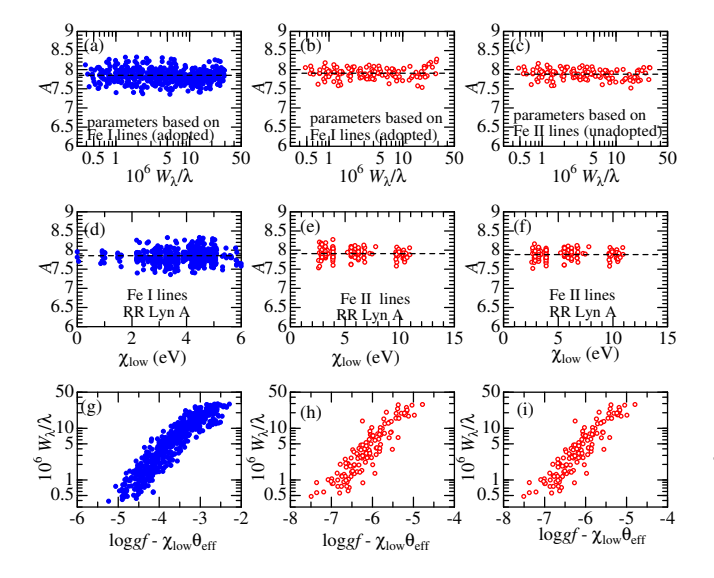


**Figure 5**. Fe abundances  $(A_i)$  of RR Lyn A corresponding to two kinds of  $(T_{\rm eff}, \nu_{\rm t})$  solutions are plotted against the reduced equivalent width  $(10^6W_{\lambda}/\lambda)$ ; top panels) or lower excitation potential  $(\chi_{\rm low})$ ; middle panels). Left and center panels correspond to the  $\sigma_1$ -minimum solutions based on Fe I lines (finally adopted), while the right panels correspond to  $\sigma_2$ -minimum solutions based on Fe II lines (which were not adopted after all). The mean abundance  $(\langle A \rangle)$  is also indicated by the horizontal dashed line. In the bottom panels are shown the corresponding empirical curves of growth, where  $\log gf - \chi_{\rm low}(5040/T_{\rm eff})$  is taken as the abscissa. The results for Fe I and Fe II lines are distinguished by blue filled circles and red open circles, respectively.

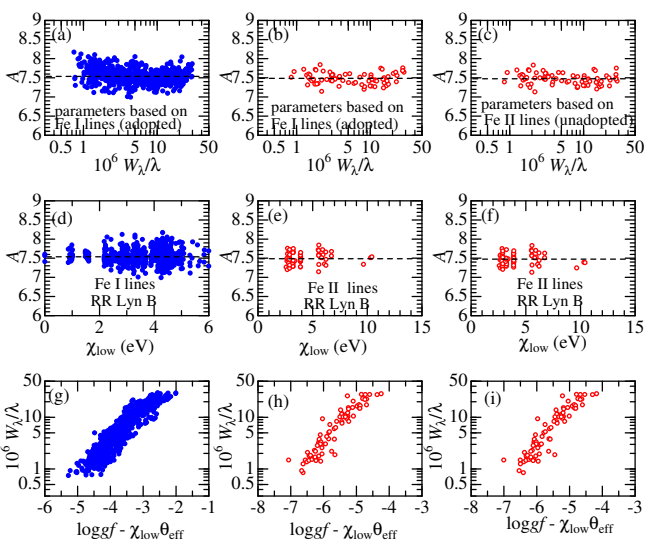


**Figure 6.** The results of Fe abundances  $(A_i)$  for RR Lyn B are presented. The left and center panels correspond to  $\sigma_1$ -minimum solutions of  $(T_{\rm eff}, v_t)$  based on Fe I lines (finally adopted), while the right panels are for the  $\sigma_2$ -minimum solutions based on Fe II lines (which were not adopted). Otherwise, the same as in Fig. 5.

**Table 3.** Adopted atmospheric parameters.

Star	$T_{ m eff}$	$v_{\rm t}$	$\log g^{\#}$	
	(K)	$(km s^{-1})$	(dex)	
A	7990	3.5	3.90	
	$(\pm 200)$	$(\pm 0.3)$	$(\pm 0.05)$	
В	7570	2.6	4.20	
	$(\pm 200)$	$(\pm 0.2)$	$(\pm 0.05)$	

Given here are the model atmosphere parameters (based on the solutions obtained from Fe I lines; cf. Table 2) finally adopted for deriving the chemical abundances of RR Lyn A and B. Parenthesized values are the roughly assigned uncertainties, which are based on the simulated random errors for  $T_{\rm eff}$  and  $\log g$  (cf. Table 2) and from the  $\log g$  errors of a few hundredths dex given by Khaliullin et al. (2001).  $^{\#}g$  is in cm s<sup>-2</sup>.

## 4. Abundance determination

## 4.1 Direct and synthetic equivalent widths

Based on the model atmospheres with the atmospheric parameters established in Section 3.4 (Table 3), elemental abundances of A and B are determinable from the equivalent widths  $(W_{\lambda})$ .

However, since identification and  $W_{\lambda}$  measurement by Gaussian fitting done in Section 2.2 was restricted to single-component lines without any serious blending with other lines, multi-component lines (e.g., Li I 6708 or Ba II 5854) or important lines appreciably blended with other features could not be included.

Therefore, an alternative synthetic spectrum-fitting approach was additionally applied to selected line features to evaluate the relevant  $W_{\lambda}$  (corresponding to the target species) inversely from the resulting abundance. Regarding the details of this alternative  $W_{\lambda}$ -determination approach, Sect. 4 of Takeda et al. (2018) may be consulted. This synthetic fitting analysis was conducted for 36 regions in total. Fig. 7 illustrates the demonstrative examples of selected 12 regions.

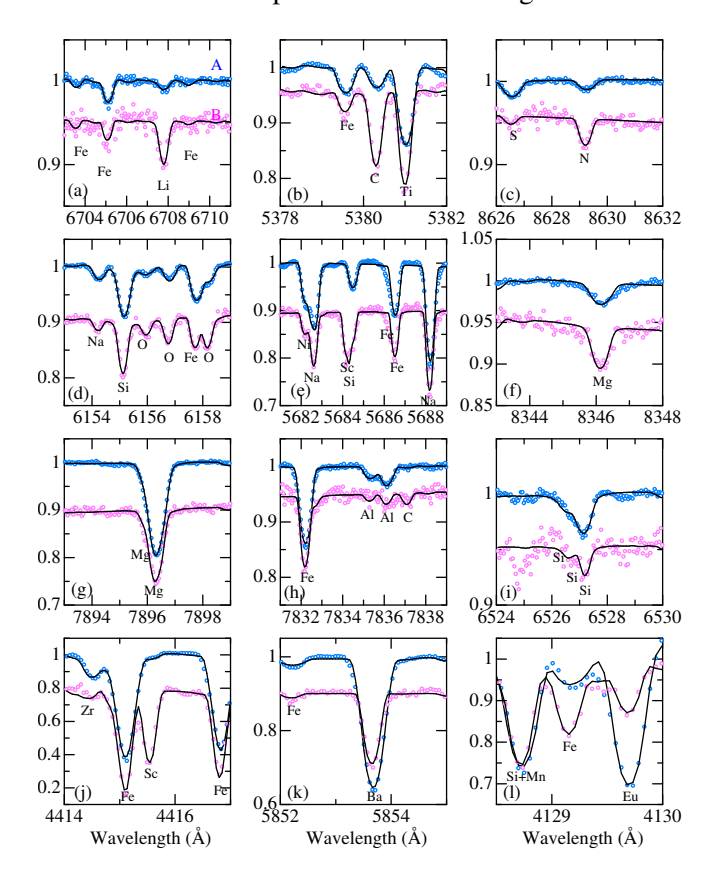


**Figure 7**. The accomplished fit of the synthetic spectrum-fitting analysis carried out for the purpose of inversely evaluating the equivalent widths. Shown here are the demonstrative results for 12 selected regions, each of which include the following target lines: (a) Li I 6708, (b) C I 5380, (c) N I 8629, (d) O I 6156/6157/6158, (e) Na I 5682/5688, (f) Mg I 8346, (g) Mg II 7896, (h) Al I 7835/7836, (i) Si I 6527, (j) Sc II 4415, (k) Ba II 5854, and (l) Eu II 4130. The observed and theoretical spectra are depicted by symbols (blue for A, pink for B) and black lines, respectively. As in Fig. 2, the scale marked in the ordinate is for A, since the spectra for B are shifted downwards by appropriate amounts (0.05 or 0.1 or 0.2).

#### 4.2 Non-LTE calculations

According to the policy of taking the non-LTE effect into consideration wherever possible, non-LTE abundances were derived for comparatively lighter elements ( $Z \le 20$  and Z = 30), for which the author already has experiences of non-LTE calculations. For other elements ( $Z \ge 21$  except for Zn) the abundances were derived under the assumption of LTE. The finally adopted (input) abundances in the calculations (and the related papers) are summarized in Table 4.

Regarding silicon (Si, Z=14), although its non-LTE calculation was carried out by Takeda (2022) in his analysis of Si II 6347/6371 doublet lines in A- and B-type stars, the atomic model used therein (34 Si I terms up to 58893 cm<sup>-1</sup> with 222 Si I radiative transitions) did not comprise sufficient number of high-excitation Si I levels, because neutral Si I lines were outside of the subject in that paper. Given the necessity of analyzing many Si I lines in this study, the atomic model for Si I was upgraded to 102 Si I terms (up to 63945 cm<sup>-1</sup>) with 1555 Si I radiative transitions. Other details of the model atom (e.g., Si II model, photoionization or collisional rates) are the same as described in Sect. 4 of Takeda (2022).

Table 4. Non-LTE calculations done in this study.

Elem. Z	# [X/H]	* [X/H]*	References <sup>†</sup>
Li 3	-0.4	0.0	Takeda & Kawanomoto (2005)
C 6	-0.8	-0.3	Takeda (1992)
N 7	-1.1	-0.6	Takeda (1992)
0 8	-0.9	-0.4	Takeda (2003)
Na 1	1 +0.2	-0.2	Takeda & Takada-Hidai (1994)
Mg 1:	2 -0.3	-0.3	Takeda (2025) (Paper II)
Al 1	3 +0.4	-0.2	Takeda (2023)
Si 1	4 +0.1	-0.1	Takeda (2022) <sup>‡</sup>
S 1	5 +0.2	+0.1	Takeda et al. (2005)
K 1	9 -0.1	-0.3	Takeda et al. (1996)
Ca 2	-0.3	0.0	Takeda (2020)
Zn 3	0 +0.9	+0.1	Takeda et al. (2005)

<sup>#</sup>Atomic number.

## 4.3 Abundance results

By inspecting the list of identified/measured lines prepared in Sect. 2.2 (or the list of selected lines defined in

<sup>\*</sup>Abundances (relative to the solar composition) assigned in non-LTE calculations for each star (in dex), which were (iteratively) chosen so that they may be almost consistent with the final results of non-LTE abundances.

<sup>&</sup>lt;sup>†</sup>These papers (and the references quoted therein) may be consulted for more details about the calculations (e.g., adopted model atoms).

<sup>‡</sup>See also Sect. 4.2.

Sect. 3.2 for Fe), we focus on the following 39 species of 30 elements: Li I, C I, N I, O I, Na I, Mg I, Mg II, Al II, Al II, Si I, Si II, S I, K I, Ca I, Ca II, Sc II, Ti II, Ti II, V I, V II, Cr I, Cr II, Mn I, Mn II, Fe I, Fe II, Co I, Ni I, Zn I, Cu I, Se I, Sr II, Y II, Zr II, Ba II, La II, Ce II, Nd II, and Eu II. Here, the lines to be adopted are restricted to only those for which  $W_{\lambda}$  values of "both A and B" are measured and available, because of an intention of line-by-line differential analysis.

Based on the equivalent widths of these selected lines (derived either by direct measurement or synthetic fitting), the abundances of relevant elements were determined by using Kurucz's (1993) WIDTH9 program, which was considerably modified by the author (e.g., treatment of merged multi-component features, taking into account the non-LTE effect, etc.). All atomic data were taken from VALD (Ryabchikova et al. 2015), except for the Li i 6708 feature for which the recipe described in Sect. 2.2 of Takeda & Kawanomoto (2005) was followed (but neighboring molecular lines were not included). The resulting detailed line-by-line abundances for A and B (with non-LTE corrections if available) and their line-averaged abundances, along with the corresponding  $W_{\lambda}$  and atomic data of spectral lines, are presented in "abundances.txt" of the online material.

Further, in deriving the mean abundances, the data of strong lines satisfying  $10^6 W_{\lambda}/\lambda > 30$  were excluded for the same reason as mentioned in Sect. 3.2 for the case of Fe lines in the determination of  $(T_{\rm eff}, \nu_{\rm t})$ .

Table 5 presents the mean results averaged over the available lines for each species:  $\langle [X/H]_A \rangle$  or  $\langle [X/H]_B \rangle$  (mean abundance relative to the Sun; i.e., line-average of  $A_i - A_\odot$ ), and  $\langle \Delta A_{A-B}^X \rangle$  (mean of line-by-line difference between A and B; i.e., line-average of  $A_{i,A} - A_{i,B}$ ). The reference solar abundances  $(A_\odot)$ ; given in the 4th column of Table 5) were mostly taken from Anders & Grevesse (1989)<sup>3</sup> in order to maintain consistency with the author's previous studies. The exceptions are 3.28 for Li (solar system abundance taken from Lodders 2003) and 7.50 for Fe (currently accepted value for the solar photosphere).

The sensitivities of abundance results to changing the atmospheric parameters ( $T_{\rm eff}$ ,  $v_{\rm t}$ , and  $\log g$ ) are also presented in Table 5, where we can see from this table that the impact of  $T_{\rm eff}$  is more significant than the

other two. That is, abundance errors due to uncertainties in  $T_{\rm eff}$  ( $\sim \pm 200$  K; cf. Table 3) are  $\lesssim 0.1$ – 0.2 dex, while those due to  $v_{\rm t}$  ( $\pm 0.3$  km s<sup>-1</sup>) as well as  $\log g$  ( $\pm 0.05$  dex) are only a few hundredths dex in most cases (note that the  $\Delta$  values given in Table 5 correspond to perturbations of  $T_{\rm eff}$  by 300 K,  $v_{\rm t}$  by 0.3 km s<sup>-1</sup>, and  $\log g$  by 0.1 dex; i.e., somewhat larger compared to above-mentioned ambiguities regarding  $T_{\rm eff}$  and  $\log g$ ).

## 5. Discussion

# 5.1 *Impact of new T*<sub>eff</sub> *and v*<sub>t</sub>

We first discuss the results of  $T_{\rm eff}$  and  $v_{\rm t}$ , which were spectroscopically established based on Fe lines (Sect. 3), in comparison with those employed in the past studies (cf. Table 1).

Regarding the effective temperature, since previous papers reported values in the ranges of  $T_{\rm eff,A} \sim 7600-8200~\rm K$  and  $T_{\rm eff,B} \sim 6900-7600~\rm K$ , our results of 7990 K (A) and 7570 K (B) rather belong to the high-scale group among the literature values.

As to the microturbulence, our  $v_{t,A}$  of 3.5 km s<sup>-1</sup> corresponds to the low-scale group among the published values ( $\sim 3-7$  km s<sup>-1</sup>), while  $v_{t,B}$  of 2.6 km s<sup>-1</sup> is almost the mean of previous determinations (2.1–3.2 km s<sup>-1</sup>)

In order to demonstrate that abundance determinations may be significantly affected by  $T_{\rm eff}$  and  $v_{\rm t}$ , we compare the adopted parameters as well as the resulting metallicity in Paper I ( $T_{\rm eff.A}/T_{\rm eff.B}$ ,  $v_{\rm t,A}/v_{\rm t,B}$  and [Fe/H]<sub>A</sub>/[Fe/H]<sub>B</sub>) = (7570/6980, 3.8/3.1, +0.11/-0.41) with those derived in this study (7990/7570, 3.5/2.6, +0.37/ - 0.01). The reason why the new [Fe/H] values in this investigation have appreciably increased by ~0.3–0.4 dex for both A and B in comparison with Paper I is due to the increase in  $T_{\rm eff}$  by ~ 400–600 K and to the decrease in  $v_{\rm t}$  by ~ 0.3–0.5 km s<sup>-1</sup>, because both act in the direction of increasing  $A({\rm Fe})$  as can be seen in columns 12–15 of Table 5).<sup>4</sup>

 $<sup>\</sup>overline{^3}$ These data may be somewhat outdated for some elements as compared to more recent compilations. For example, Asplund et al.'s (2009) solar CNO abundances (derived by taking into account the 3D effect) are by  $\sim 0.2$ –0.3 dex lower than the values adopted here. Note, however, that the solar CNO abundances derived from the classical 1D plane-parallel atmosphere by including the non-LTE effect (such as done in this study) are rather consistent with those of Anders & Grevesse (1989) adopted here (cf. Takeda 1994).

<sup>&</sup>lt;sup>4</sup>It was mentioned in Sect. 4.3 that the effect of changing  $v_t$  on the abundances is not so significant (in contrast to the case of changing  $T_{\rm eff}$ ). It should be noted, however, that this is due to the specific situation in this study: (i) a large number of weak Fe lines (for which the resulting abundances hardly depend upon  $v_t$ ) could be employed and (ii) strong lines satisfying  $10^6W_\lambda/\lambda > 30$  were excluded in deriving the mean abundance. Generally, changing  $v_t$  (even by only a few tens km s<sup>-1</sup>) may bring about appreciable variations in the resulting abundances depending on the lines used in the analysis.

## 5.2 Trends of chemical abundances

Based on the results in Table 5,  $\langle [X/H]_A \rangle$ ,  $\langle [X/H]_B \rangle$ , and  $\langle \Delta A_{A-B}^X \rangle$  are plotted against Z in Fig. 8a, 8b, and 8c, respectively. Considering the impact of uncertainties in atmospheric parameters (cf. Table 3 and Table 5) and the size of standard deviations in the averages (cf. "abundances.txt"), typical statistical errors involved with the data symbols in Fig. 8 may be estimated as  $\pm \lesssim 0.1$ –0.2 dex. While some additional systematic errors can not be ruled out in [X/H] values related to other factors (e.g., reference solar abundances, gf values, non-LTE effect for  $Z \ge 21$  elements, etc.),  $\Delta A_{A-B}^X$  values (line-by-line differential abundances) should be almost irrelevant to such systematic error sources because of being almost canceled out.

Several notable features are observed by inspecting Fig. 8 as summarized below (the symbols "\" and "\" to indicate average values are omitted for simplicity):

- Roughly speaking, [X/H] (departure from the solar composition) tends to increase with Z in the global sense for both A and B (Fig. 8a and 8b); i.e.,  $[X/H]_A < 0$  at  $Z \le 10$ ,  $[X/H]_A \sim 0$  at  $10 \le Z \le 20$ , and  $[X/H]_A > 0$  at  $Z \ge 20$  for RR Lyn A; while  $[X/H]_B < 0$  at  $Z \le 10$ ,  $[X/H]_B \sim 0$  at  $[X/H]_B \sim 0$  at [X/H
- We have confirmed that A is an Am star, which shows typical characteristics of Am phenomenon (e.g., underabundances of CNO, moderate enrichment of Fe-group elements, and large overabundances of s-process elements and rare earths). However, the drastic depletion of Sc ([Sc/H]<sub>A</sub> ~ −1.6) is worth noting, which is rather puzzling because the deficiency of Ca (considered to conform with Sc in Am stars) is only mild ([Ca/H]<sub>A</sub> ~ −0.3). This problem is separately discussed in Sect. 5.4.
- In contrast, chemical aberrations of B are only marginal: rather tight and gradual Z-dependence of [X/H]<sub>B</sub>, while [X/H] ~ 0 for elements of intermediate Z (such as Fe group). Therefore, B may be classified as a weak Am star of almost solar metallicity.

## 5.3 RR Lyn B is not metal-deficient

While the conclusion of metal-rich nature for RR Lyn A is more or less consistent with most of the past publications, our finding that "RR Lyn B is a solar-metallicity star ( $[Fe/H]_B \sim 0$ ) with a gradually increasing trend

of [X/H]<sub>B</sub> with Z' is significant, because it apparently conflicts with the results of previous investigations, most of which concluded B to be of subsolar metallicity (cf. Table 1).

- Kondo (1976) mentioned that Fe is likely to be deficient in B.
- Lyubimkov & Rachkovskaya's (1995b) separate analysis for A and B (based on CCD spectra) yielded [Fe/H]<sub>B</sub> = -0.33, from which they concluded that B may be a λ Boo star of metal-deficient peculiarity.
- Burkhart & Coupry (1991) reported  $[Fe/H]_B = -0.3$ , though details of their analysis (e.g.,  $v_t$ ,  $\log g$ ) are not described.
- Hui-Bon-Hoa (2000) derived  $[Fe/H]_B = -0.19$ , though with a remark of "uncertain value".
- Khaliullin et al. (2001) obtained [Fe/H]<sub>B</sub> = -0.24(±0.06), though this is a photometric metallicity derived from the length of the blanketing vector in two-color diagram.
- Jeong et al. (2017) concluded rather confidently based on their abundance determinations that B ( $[Fe/H]_B = -0.33$ ) is a  $\lambda$  Boo star, because they observed characteristic abundance differences between volatile (low condensation temperature  $T_c$ ) and refractory (high  $T_c$ ) elements; i.e., they found that the former is almost solar but the latter is appreciably deficient (cf. their Fig. 4B).

Since the discrepancy of [Fe/H]<sub>B</sub> between Paper I (-0.41) and this study (-0.01) can be reasonably explained by the difference in  $T_{\text{eff}}$  and  $v_{\text{t}}$  (cf. Sect. 5.1), the atmospheric parameters adopted by these authors were examined. It was then found that the values of  $T_{\text{eff},B}$  adopted in most of these papers are appreciably lower than ours (7570 K) by  $\sim 400-700$  K: 6900 K (Kondo 1976), 7150 K (Lyubimkov & Rachkovskaya 1995b), 6980 K (Khaliullin et al. 2001), 7210 K (Jeong et al. 2017); though Burkhart & Coupry (1991) and Hui-Bon-Hoa (2000) employed ~ 7500-7600 K like this study. Therefore, in view of the significant role of  $T_{\rm eff}$  in abundance derivation (cf. Sect. 5.1), we suspect that the apparently subsolar metallicity of RR Lyn B concluded by these authors may be mainly due to their use of inadequately low  $T_{\rm eff}$ .

The systematic trend of  $[X/H]_B$  in terms of  $T_c$ , which was reported by Jeong et al. (2017) as an evidence for a  $\lambda$  Boo star, is not observed in our analysis. This can be recognized in Fig. 9, where our abundance results in Table 5 are plotted against  $T_c$ . It is apparent

that such a  $T_{\rm c}$ -dependent trend in [X/H]<sub>B</sub> with a negative slope as found by Jeong et al. (2017; cf. their Fig. 4B) is absent in our [X/H]<sub>B</sub> results (cf. Fig. 9b; the trend is even the contrary to their claim, because the slope is rather positive). Although several factors may be involved with this disagreement (e.g., difference in atmospheric parameters, their neglect of non-LTE effect for volatile elements, etc.), much can not be said unfortunately, because sufficient details of the spectral lines they used are not presented.

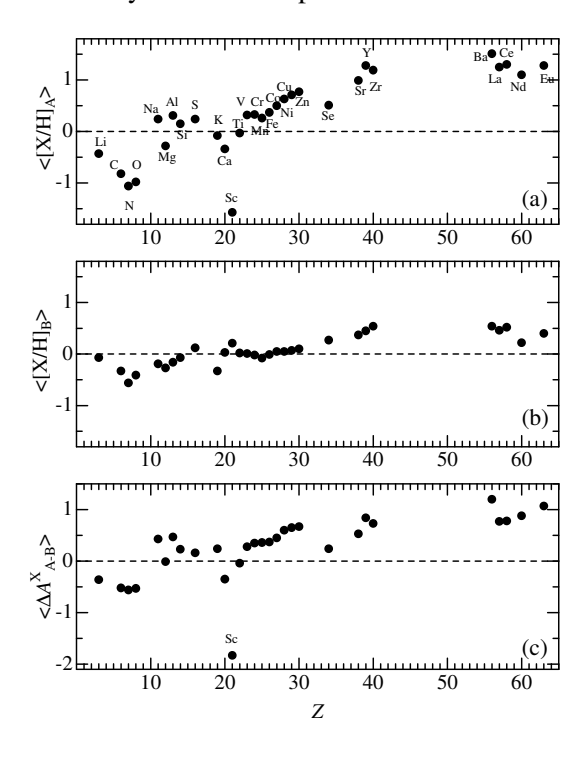


**Figure 8.** Plotted against Z (atomic number) are (a)  $\langle [X/H]_A \rangle$  (averaged differential abundance of element X relative to the Sun for RR Lyn A), (b)  $\langle [X/H]_B \rangle$  (ditto for RR Lyn B), and (c)  $\langle \Delta A_{A-B}^X \rangle$  (averaged line-by-line differential abundance of element X between A and B), for 30 elements based on the data in Table 5. Regarding the elements where two results of different ionization stages are available (Mg, Al, Si, Ca, Ti, Cr, Mn, Fe), their mean values are adopted here (exceptionally, the result for V II is used for V because that for V I based on only one line is appreciably discrepant).

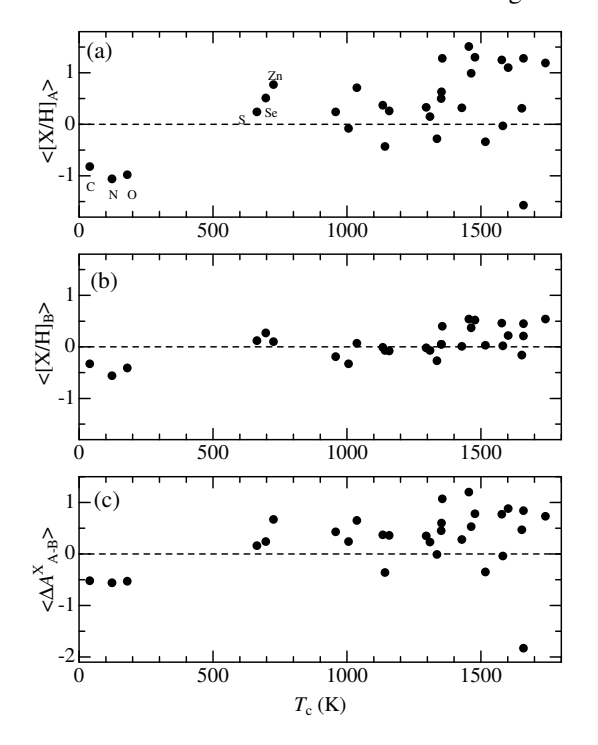


**Figure 9.** The results of (a)  $\langle [X/H]_A \rangle$ , (b)  $\langle [X/H]_B \rangle$ , and (c)  $\langle \Delta A_{A-B}^X \rangle$  derived for 30 elements are plotted against  $T_c$  (50% condensation temperature). Otherwise, the same as in Fig. 8.

## 5.4 Scandium problem in RR Lyn A

It is remarkable that  $Sc\ (Z=21)$  shows a conspicuously large underabundance ([Sc/H] = -1.6) in RR Lyn A, which markedly deviates from the global trend of [X/H] distributing around  $\sim 0$  (within  $\pm$  several tenths dex) for  $10 \lesssim Z \lesssim 25$  elements (Fig. 8a). It is worth noting that  $Ca\ (Z=20)$  is only mildly subsolar (by  $\sim -0.3$  dex) and does not conform to the substantial deficiency of Sc. This is somewhat strange, because Ca and Sc are considered to behave similarly in Am stars, where weak  $Ca\ \pi$  and/or  $Sc\ \pi$  lines (along with enhanced strengths of heavy metal lines) are their discovery criteria in spectral classifications (cf. Table 1 in Preston 1974). Actually, according to Fig. 5 of Smith's (1996) review paper, published results of [Ca/H] and [Sc/H] appear to be rather similar in Am–Fm stars.

In order to examine whether such a striking abundance difference between Sc and Ca could be possible in Am stars, Sc abundances of 101 (mostly A-type) stars studied by Takeda et al. (2018) were determined from the Sc II 5526 line, and compared them with the Ca abundances derived from the Ca I 6162 line. This supplementary analysis is separately described in Appendix A.

It was then found as the characteristic trend of Am stars that (i) [Sc/H] and [Ca/H] positively correlate

with each other and (ii) the gradient d[Sc/H]/d[Ca/H] is greater than 1 (Fig. 10c), which means that the extent of deficiency is larger for Sc than for Ca ( $||Sc/H|| \gtrsim ||Ca/H|||$ ). Although the ratio of [Sc/H]/[Ca/H]  $\simeq 4-5$  found for RR Lyn A appears somewhat too large compared to other Am stars (typically around  $\sim 2$ ), it might be regarded as a result of random scatter because the correlation becomes progressively diversified as the deficiency is enhanced. Accordingly, we may state that the markedly large discordance between [Sc/H] and [Ca/H] observed in RR Lyn A is qualitatively understandable within the framework of the general characteristics of Am stars, though it is a rather rare phenomenon in the quantitative sense.

From the viewpoint of the theoretical side, a number of researchers have devoted efforts to elucidating the cause of Am phenomenon over the past half century. Above all, chemical segregation (element diffusion) coupled with mass loss, which may take place in the stable atmosphere/envelope has been regarded as a promising mechanism, though the abundance behaviors Ca and Sc in Am stars are not yet successfully explained by the diffusion theory (see Michaud et al. 2015; and the references therein). Alternatively, some authors considered another possibility for the origin of Am anomalies, such as due to accretion of interstellar matter coupled with charge-exchange reactions (Böhm-Vitense 2006; Jeong et al. 2017).

In any event, these remarkable features revealed from this study (i.e., very discordant abundance deficiency between Sc and Ca in RR Lyn A, while almost normal Ca and even somewhat supersolar Sc in RR Lyn B of lower  $T_{\rm eff}$  by only  $\sim 400$  K) would serve as a valuable observational constraint and an ideal testing bench for any theory challenging to explain the chemical peculiarities in Am stars, because stellar parameters (including the age of  $\sim 1 \times 10^9$  yr; Khaliullin et al. 2001) are well established for both components.

## 6. Summary and conclusion

RR Lyn A+B is an eclipsing binary system (with orbital period of  $\sim 10$  d) consisting of two main-sequence stars, in which the hotter A is classified as an metallicline A-type star. Several previous investigations reported that surface abundances of these two components are considerably different from each other (i.e., A is metal-rich but B is even metal-poor) despite that both should have born with the same chemical composition.

Therefore, this system may be regarded as an important key to clarify the physical mechanism triggering chemical peculiarities (Am phenomenon) in

the stellar surface by carefully examining the detailed abundances of various elements for both components.

However, extensive elemental abundance study for both A and B based on high-quality data are still insufficient, reflecting the difficulty of analyzing complex double-lined spectra of RR Lyn. Besides, atmospheric parameters (especially  $T_{\rm eff}$  and  $v_{\rm t}$ ), which may significantly affect abundance determinations, are not yet reliably established, because appreciably diversified values have been reported in the past studies.

Motivated by this situation, the purpose of this study was to carry out a detailed spectroscopic study of RR Lyn A+B in order to determine the key atmospheric parameters and elemental abundances of A and B as precisely as possible and to examine how they compare with each other.

Regarding the basic observational data, the spectrum-disentangle technique was applied to a set of double-line spectra taken at different orbital phases to obtain the decomposed spectra of A and B. Based on these disentangled spectra (covering 3900–9200 Å), many lines judged to be usable were identified and their  $W_{\lambda}$  were measured by the direct Gaussian-fitting. In addition,  $W_{\lambda}$  values of important line features (even if they are blended with other lines or consist of complex multi-components) were evaluated by applying the spectrum-synthesis technique.

The values of  $(T_{\rm eff}, v_{\rm t})$  were determined from many Fe I lines by requiring that abundances do not show any systematic dependence upon  $W_{\lambda}$  and  $\chi_{\rm low}$ , where stronger lines  $(10^6W_{\lambda}/\lambda > 30)$  had to be discarded because they turned out to behave anomalously. This analysis yielded (7990 K, 3.5 km s<sup>-1</sup>) and (7570 K, 2.6 km s<sup>-1</sup>) for A and B, respectively.

The chemical abundances of 30 elements (39 species) were derived from the  $W_{\lambda}$  values of many lines, where the non-LTE effect was taken into account for comparatively lighter elements ( $Z \le 20$  and Z = 30). The following characteristics were found in the resulting  $[X/H]_A$  and  $[X/H]_B$ .

- Roughly speaking, [X/H] tends to increase with Z for both A and B. That is, light elements (Z < 10) are subsolar, intermediate elements  $(10 \le Z \le xx)$  are nearly solar; and heavy elements  $(xx \le Z)$  are supersolar, where  $xx \sim 20$  for A and  $xx \sim 30$  for B. These are the characteristic trends observed in Am stars.
- Abundance peculiarities are quantitatively more conspicuous in A than in B, resulting in a similar increasing trend with Z also for the differential abundances between A and B (ΔA<sup>X</sup><sub>A-B</sub>).
- Yet, regarding the hotter A, Sc shows a strikingly large deficiency ( $[Sc/H]_A \simeq -1.6$ ) deviat-

ing the global trend. Although it is somewhat strange that Ca is only mildly underabundant ( $[Ca/H]_A \sim -0.3$ ) and does not conform to Sc (since both are considered to behave similarly), such a large discordance may not necessarily be improbable, since Sc tends to be more deficient than Ca in Am stars.

– It is significant that the abundances of iron group elements ( $20 \le Z \le 30$ ) in RR Lyn B are almost solar ([Fe/H]<sub>B</sub>  $\simeq 0.0$ ). This conclusion is in contrast with the results of previous studies, most of which reported that B is metal-deficient (such as like  $\lambda$  Boo stars) by several tenths dex. This discrepancy may be attributed to the difference in the adopted atmospheric parameters (e.g.,  $T_{\rm eff}$ ).

In short, RR Lyn A is a typical (classical) Am star of supersolar metallicity ([Fe/H]<sub>A</sub>  $\simeq$  +0.4) with a conspicuously large Sc deficiency. Meanwhile, RR Lyn B is a solar-metallicity star ([Fe/H]<sub>B</sub>  $\simeq$  0.0) with a trend of [X/H]<sub>B</sub> gradually increasing with Z (i.e., a nearnormal star accompanied by weak Am characteristics). It is thus important to elucidate the reason why such dissimilar types of chemical anomalies are observed in A and B (with a small  $T_{\rm eff}$  difference of  $\sim$  400 K), for which challenges of theoreticians are awaited.

## Appendix A. Sc and Ca abundances of A-type stars

In view of the remarkably large underabundance of Sc found in RR Lyn A ( $\sim -1.6$  dex) despite of only a mild deficiency ( $\sim -0.3$  dex) of Ca (which is considered to behave along with Sc in Am stars), it is worth examining the trends of Sc and Ca abundances and their mutual correlations in a large sample of A-type stars, in order to see whether such a substantial difference between Sc and Ca is possible in Am stars.

Conveniently, Takeda et al. (2018) once carried out CNO abundance determinations for 101 main-sequence stars (in the parameter ranges of  $0 \le v_e \sin i \le 100 \text{ km s}^{-1}$  and  $7000 \le T_{\text{eff}} \le 10000 \text{ K}$ ), most of which are A-type stars including 25 Am stars (i.e., classified as Am in Hipparcos catalogue; cf. Sect. 2 in Takeda et al. 2018). Therefore, Sc abundances of these 101 stars were determined (in LTE) by applying the spectrum-fitting technique to the wavelength region comprising the Sc II 5526.79 line ( $\chi_{\text{low}} = 1.768 \text{ eV}$ ,  $\log gf = +0.024$ ) based on the same observational data and the same atmospheric parameters as adopted therein.

Although abundance solutions were successfully converged for most cases (excepting 5 stars), a possibility of converging at a spurious solution still remains,

especially for broad-line cases of larger  $v_e \sin i$ . Therefore, the credibility of the resulting abundance was assessed as follows. The equivalent width of the Sc II 5526 line ( $W_{5526}$ ) was calculated from the fitting-based abundance as done in Sect. 4.1. Meanwhile, the critical line strength at the detectability limit may be roughly estimated as  $W_* \simeq h \times \epsilon$ , where h is the full-width at the half maximum of the line (evaluated from  $v_e \sin i$ ) and  $\epsilon$  is the minimum-detectable line-depth depending upon SNR (signal-to-noise ratio) as  $\epsilon \simeq 1/\text{SNR}$ . If  $W_{5526}$  was smaller than  $W_*$ , then the abundance was judged to be unreliable. Besides, for the unsuccessful cases where fitting solutions failed to converge, the upper-limit abundances ware derived from  $W_*$ .

The Ca abundances (in LTE) of 101 stars were actually derived (though the results were not published) in the study of Takeda et al. (2018) by the fitting analysis of the 6146–6163 Å region (see Fig. 4 therein) including the Ca I 6162.16 line ( $\chi_{low}=1.899$  eV,  $\log gf=+0.100$ ). The reliabilities of these Ca abundances were assessed in the same manner as done for Sc.

Thus obtained Sc and Ca abundances of 101 stars are summarized in "scabund101.txt" of the online material. Their dependence upon  $T_{\rm eff}$  or  $v_{\rm e} \sin i$  as well as mutual correlations are illustrated in Fig. 10, where the spectrum fitting in the Sc II 5526 line region for two representative stars (Am star HD 072037 and non-Am star HD 189849) is also demonstrated (Fig. 10f). In addition, since Mashonkina & Fadeyev (2024) recently determined Ca and Sc abundances for a number of A-type stars by taking into account the non-LTE effect. their non-LTE A(Ca) and A(Sc) values (taken from their Table 1 and Table 2) are also overplotted in this figure for comparison. The following characteristics are observed from this figure regarding the Sc and Ca abundances of Am stars.

- The abundances of both elements are generally subsolar in Am stars by several tenths to  $\sim 1$  dex, though the dispersion for Sc (-1.5  $\lesssim$  [Sc/H]  $\lesssim$  0) is somewhat larger than that for Ca (-1  $\lesssim$  [Ca/H]  $\lesssim$  0) (Fig. 10a and 10d).
- A weak  $v_e \sin i$ -dependent trend is seen for both Sc and Ca in Am stars, in the sense that slower rotators tend to show larger deficiencies (Fig. 10b and 10e).
- A(Sc) and A(Ca) are positively correlated with each other, though the dispersion tends to be larger with the dA(Sc)/dA(Ca) gradient being steeper (> 1) towards increasing the deficiency in Am stars (Fig. 10c).
- The non-LTE results of A(Ca) and A(Sc) derived

by Mashonkina & Fadeyev (2024) are almost in accord with the present LTE results as seen from Fig. 10a–10e. Though their A(Ca) values tend to be somewhat higher in the strict sense, the same overall trends are observed.

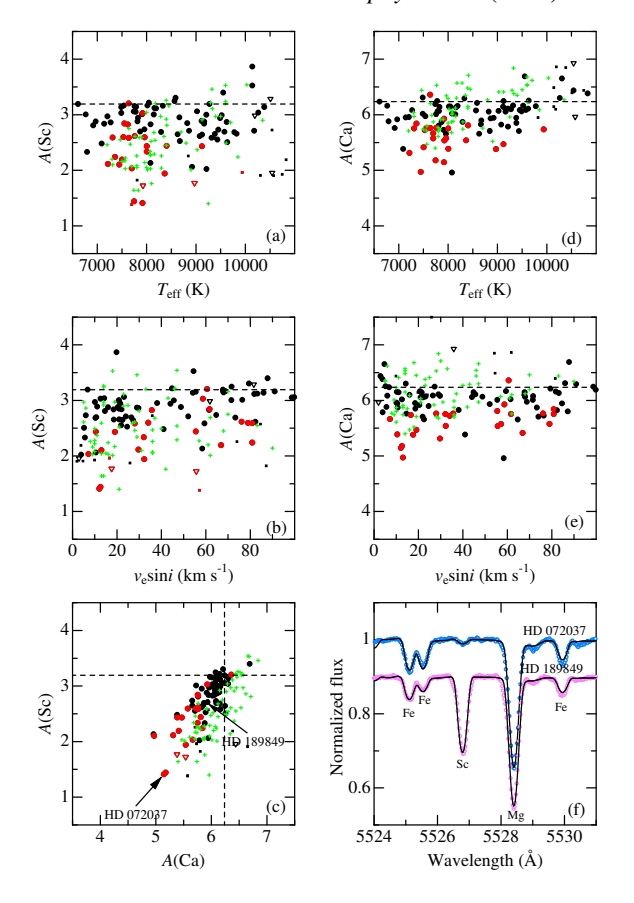


Figure 10. Trends and correlations of Sc and Ca abundances determined for 101 sharp-lined (mostly) A-type stars. In panels (a), (b), (d), and (e) are plotted the abundances of A(Sc) (left) and A(Ca)(right) against  $T_{\text{eff}}$  (top) and  $v_{\text{e}} \sin i$  (middle). The correlation between A(Sc) and A(Ca) is illustrated in panel (c). Panel (f) demonstrates the spectrum fitting in the region comprising the Sc II 5526 line for two representative cases of HD 072037 and HD 189849 (depicted in the same manner as in Fig. 7). In each panel showing A(Sc) or A(Ca), ordinary data, unreliable data, and upper limits (indeterminable cases) are denoted by filled circles, small dots, and open downward triangles, respectively. The data for Am stars (25 out of 101 stars) are highlighted in red. The abundances of the reference star Procyon (HD 061421) (3.19 for Sc and 6.24 for Ca; which may be regarded as good proxies for the solar abundances) are indicated by dashed lines. comparison, the non-LTE Ca and Sc abundances determined by Mashonkina & Fadeyev (2024), which were taken from their Table 1 and Table 2, are also overplotted by light-green crosses in panels (a)–(e).

## Acknowledgements

Data analysis (numerical calculation of spectrum disentangling) was carried out on the Multi-wavelength

Data Analysis System operated by the Astronomy Data Center (ADC), National Astronomical Observatory of Japan. This investigation has made use the VALD database operated at Uppsala University, the Institute of Astronomy RAS in Moskow, and the University of Vienna.

#### Online materials

This article accompanies the following online materials (electronic data files). See "ReadMe.txt" for the details about their contents.

- ReadMe.txt
- specdata\_A.txt
- specdata\_B.txt
- ewlines\_A.txt
- ewlines\_B.txt
- abundances.txt
- scabund101.txt

#### References

- Anders, E., & Grevesse, N. 1989, Geochim. Cosmochim. Acta, 53, 197
- Asplund, M., Grevesse, N., Sauval, A. J., & Scott, P. 2009, ARA&A, 47, 481
- Böhm-Vitense, E. 2006, PASP, 118, 419
- Burkhart, C., & Coupry, M. F. 1991, A&A, 249, 205
- Hui-Bon-Hoa, A. 2000, A&AS, 144, 203
- Jeong, Y., Yushchenko, A. V., Doikov, D. N., Gopka, V. F., & Yushchenko, V. O. 2017, J. Astron. Space Sci, 34, 75
- Khaliullin, Kh. F., Khaliullin, A. I., & Krylov, A. V. 2001, Astron. Rep., 45, 888
- Kondo, M. 1976, Annals of Tokyo Astronomical Observatory, 2nd Ser. 16, 1
- Künzli, M., & North, P. 1998, A&A, 330, 651
- Kurucz, R. L. 1993, Kurucz CD-ROM, No. 13 (Harvard-Smithsonian Center for Astrophysics)
- Lodders, K. 2003, ApJ, 591, 1220
- Lyubimkov, L. S., & Rachkovskaya, T. M. 1995a, Astron. Rep., 39, 56
- Lyubimkov, L. S., & Rachkovskaya, T. M. 1995b, Astron. Rep., 39, 63

- Mashonkina, L. I., & Fadeyev, Yu. A. 2024, Astron. Lett., 50, 373
- Michaud, G., Alecian, G., & Richer, J. 2015, Atomic Diffusion in Stars, Astronomy and Astrophysics Library (Springer International Publishing: Switzerland), Sect. 9.3.2.2
- Preston, G. W. 1974, ARA&A, 12, 257
- Rachkovskaya, T. M. 1974, Krymskaya Astrofizicheskaya Observatoriya, Izvestiya, 52, 35 (in Russian)
- Ryabchikova, T., Piskunov, N., Kurucz, R. L., Stempels, H. C., Heiter, U., Pakhomov, Yu., & Barklem, P. S. 2015, Physica Scripta, 90, 054005
- Smith, K. C. 1996, Ap&SS, 237, 77
- Smith, M. A. 1971, A&A, 11, 325
- Takeda, Y. 1992, PASJ, 44, 649
- Takeda, Y. 1994, PASJ, 46, 53
- Takeda, Y. 2003, A&A, 402, 343
- Takeda, Y. 2020, Stars & Galaxies, 3, 1 (erratum appended)
- Takeda, Y. 2022, Contrib. Astron. Obs. Skalnaté Pleso, 52, 5
- Takeda, Y. 2023, Contrib. Astron. Obs. Skalnaté Pleso, 53, 31
- Takeda, Y. 2024, Astron. Nachr., 345, e20230174
- Takeda, Y. 2025, Res. Astron. Astrophys, 25, 025016 (Paper II)
- Takeda, Y., Han, I., Kang, D.-I., Lee, B.-C., & Kim, K.-M. 2008, JKAS, 41, 83
- Takeda, Y., Han, I., Kang, D.-I., Lee, B.-C., & Kim, K.-M. 2019, MNRAS, 485, 1067 (Paper I)
- Takeda, Y., Hashimoto, O., Taguchi, H., Yoshioka, K., Takada-Hidai, M., Saito, Y., & Honda, S. 2005, PASJ, 57, 751
- Takeda, Y., Kato, K.-I., Watanabe, Y., & Sadakane, K. 1996, PASJ, 48, 511
- Takeda, Y., & Kawanomoto, S. 2005, PASJ, 57, 45
- Takeda, Y., Kawanomoto, S., Ohishi, N., Kang, D.-I., Lee, B.-C., Kim, K.-M., & Han I. 2018, PASJ, 70, 91
- Takeda, Y., & Takada-Hidai, M. 1994, PASJ, 46, 395
- Venn, K., & Lambert, D. L. 1990, ApJ, 363, 234

Table 5. Results of elemental abundances for RR Lyn A and B.

(1) (2) (3) (4) (5) (6) (7) (8) (9) (10) (11) (12) (13) (14) (15) (16) (17)		<u> </u>			3.7	/FX73 \ X7	/FX73 \ 3.7	/ 4 77	1 T ± 1 T ±	▲ 12± ▲ 12±	<u>g+</u> <u>g+</u>
Constant	$\overline{Z}$	Species	$T_{\rm c}$	$A_{\odot}$	N (5)	$\langle [X]_A \rangle N_A$	$\langle [X]_{B} \rangle N_{B}$	$\langle \Delta X_{A-B} \rangle N_{A-B}$	$\Delta_{\rm A}^{T+}$ $\Delta_{\rm B}^{T+}$	$\Delta_{A}^{v+}$ $\Delta_{B}^{v+}$	$\Delta_{\rm A}^{g+}$ $\Delta_{\rm B}^{g+}$
S	(1)	(2)	(3)	(4)	(5)				(12) (13)	(14) (15)	(10) (1/)
6 C <sub>1</sub> 40 8.56 25 -0.82 (23) -0.33 (20) -0.52 (20) +03-03 -01-01 +01+02 7 N <sub>1</sub> 123 8.05 7 -1.06 (6) -0.56 (6) -0.56 (7) -04-08 -00-00 +02+03 8 O <sub>1</sub> 180 8.93 9 -0.98 (7) -0.41 (8) -0.53 (7) -05-09 -01-02 +02+03 11 Na <sub>1</sub> 958 6.33 8 +0.24 (5) -0.19 (6) +0.43 (4) +11+07 -02-02 -01+00 12 Mg <sub>1</sub> 1336 7.58 18 -0.31 (13) -0.29 (13) -0.04 (12) +12+07 -01-01 -01+00 12 Mg <sub>1</sub> 1336 7.58 6 -0.25 (4) -0.25 (4) +0.01 (5) -0.3 -08 -02-01 +01 +03 13 Al <sub>1</sub> 1653 6.47 8 +0.31 (6) -0.16 (6) +0.47 (6) +13+06 -00-00 -02+01 13 Al <sub>1</sub> 1653 6.47 8 +0.31 (6) -0.16 (6) +0.47 (6) +13+06 -00-00 -02+01 14 Si <sub>1</sub> 1310 7.55 49 +0.13 (47) -0.04 (48) +0.20 (47) +11+06 -00-01 -01+01 14 Si <sub>1</sub> 1310 7.55 5 +0.17 (4) -0.09 (5) +0.25 (4) -04-09 -03-03 -03 -02-01+01 +01 +01 14 Si <sub>1</sub> 1310 7.55 5 5 +0.17 (4) -0.09 (5) +0.25 (4) -04-09 -03-03 -03 -02-01 +01 +01 +01 14 Si <sub>1</sub> 1310 7.55 5 -0.08 (1) -0.33 (1) +0.12 (11) +0.16 (12) +09+02 -01-01 +00 +02 +03 14 Si <sub>1</sub> 1310 7.55 5 -0.08 (1) -0.33 (1) +0.12 (11) +0.16 (12) +09 +02 -01-01 +00 +02 +03 14 Si <sub>1</sub> 1310 7.55 5 -0.07 (4) +0.01 (21) +0.16 (12) +09 +02 -01-01 +01 +00 +02 +03 14 Si <sub>1</sub> 1310 7.55 5 -0.17 (4) -0.09 (5) +0.25 (4) -0.4-09 -0.3-03 -03 -02 -04 +01 +01 +01 +01 +01 +01 +01 +01 +01 +01	2	11.	1142	2 20	1				±16 ±11	+00 +00	01 + 01
7 N <sub>1</sub> 123 8.05 7 -1.06 (6) -0.56 (6) -0.56 (7) -04-08 -00-00 +02+03 8 O <sub>1</sub> 180 8.93 9 -0.98 (7) -0.41 (8) -0.53 (7) -05-09 -01 -02 +02+03 11 Na <sub>1</sub> 958 6.33 8 +0.24 (5) -0.19 (6) +0.43 (4) +111+07 -02-02 -01+00 12 Mg ii 1336 7.58 18 -0.31 (13) -0.29 (13) -0.04 (12) +12+07 -01-01 -01 +00 12 Mg ii 1336 7.58 6 -0.25 (4) -0.25 (4) +0.01 (5) -0.3-08 -02-01 +01+03 13 Al ii 1653 6.47 8 +0.31 (6) -0.16 (6) +0.47 (6) +13+06 -00-00 -02+01 13 Al ii 1653 6.47 8 +0.31 (6) +0.33 (1) +0.12 (1) +0.5-10 -01-00 +02+03 14 Si ii 1310 7.55 49 +0.13 (47) -0.04 (48) +0.20 (47) +11+06 -00-01 -01+01 14 Si ii 1310 7.55 5 +0.17 (4) -0.09 (5) +0.25 (4) -0.40 (47) +11+06 -00-01 -01+01 14 Si ii 1310 7.55 5 +0.17 (4) -0.09 (5) +0.25 (4) -04-09 -03-03 +02+04 16 S1 664 7.21 13 +0.24 (11) +0.12 (11) +0.16 (12) +09+02 -01-01 +00+02 19 K1 1006 5.12 1 -0.08 (1) -0.33 (1) +0.24 (1) +13+09 -01-02 -01+00 120 Ca ii 1517 6.36 26 -0.42 (24) +0.01 (21) -0.41 (21) +15+08 -01-05 -01+01 20 Ca ii 1517 6.36 26 -0.42 (24) +0.04 (5) -0.29 (4) +0.20 -3 -04+05 +02+02 30 Zn i 726 4.60 4 +0.77 (4) +0.10 (4) +0.67 (4) +14+08 -03-02 -01+01 122 Ti ii 1582 4.99 4 -0.01 (4) +0.04 (5) -0.29 (4) +0.67 (4) +14+08 -03-02 -01+01 122 Ti ii 1582 4.99 60 -0.04 (38) +0.04 (41) -0.07 (38) +09+05 -02-03 +03 +04 23 V ii 1429 4.00 1 +0.07 (1) -0.22 (1) +0.22 (1) +18+13 -00-00 -01 -01+01 22 Ti ii 1582 4.99 60 -0.04 (38) +0.04 (41) -0.07 (38) +09+05 -02-02 3 +03 +04 24 Cr ii 1296 5.67 21 +0.23 (19) -0.08 (19) +0.31 (19) +15+10 -01-02 -01+01 24 Cr ii 1296 5.67 32 +0.43 (24) +0.01 (24) +0.05 (29) +0.40 (24) +0.5 +01 -03 -03 +03 +04 25 Mn ii 1158 5.39 11 +0.31 (1) -0.08 (1) +0.08 (1) +0.33 (1) +0.46 (25) +0.50 (1) +15 +09 -01 -02 -01+01 24 Cr ii 1296 5.67 32 +0.43 (24) +0.05 (29) +0.40 (24) +0.5 +01 -03 -03 +03 +04 25 Mn ii 1158 5.39 11 +0.31 (1) -0.08 (1) +0.05 (5) +0.45 (5) +15 +09 -01 -01 -01 -01 +01 26 Fe ii 1134 7.50 56 +0.40 (56) -0.03 (55) +0.45 (5) +0.45 (5) +15 +09 -01 -01 -01 -01 +01 29 Cu ii 1037 4.21 1 +0.71 (1) +0.07 (1) +0.05 (1) +0.65 (1) +17+12 -01 -01 -01 +01 29 Cu ii 10						, ,					
S						, ,	, ,	` '			
$\begin{array}{c ccccccccccccccccccccccccccccccccccc$						, ,		` '			
$ \begin{array}{c ccccccccccccccccccccccccccccccccccc$						, ,	, ,	` '			
12 Mg π 1336 7.58 6 -0.25 (4) -0.25 (4) +0.01 (5) -03 -08 -02 -01 +01 +03 13 Al π 1653 6.47 8 +0.31 (6) -0.16 (6) +0.47 (6) +13 +06 -00 -00 -02 +01 13 Al π 1653 6.47 1 +0.45 (1) +0.33 (1) +0.12 (1) -0.5 -10 -01 -00 +02 +03 14 Si π 1310 7.55 49 +0.13 (47) -0.04 (48) +0.20 (47) +11 +06 -00 -01 -01 +01 14 Si π 1310 7.55 5 5 +0.17 (4) -0.09 (5) +0.25 (4) -04 -09 -03 -03 +02 +04 16 S π 664 7.21 13 +0.24 (11) +0.12 (11) +0.16 (12) +09 +02 -01 -01 +00 +02 19 K π 1006 5.12 1 -0.08 (1) -0.33 (1) +0.24 (1) +13 +09 -01 -02 -01 +00 20 Ca π 1517 6.36 26 -0.42 (24) +0.01 (21) -0.41 (21) +15 +08 -01 -05 -01 +01 20 Ca π 1517 6.36 5 -0.25 (4) +0.04 (5) -0.29 (4) +0.2 -03 -03 -02 -01 +01 20 Ca π 1517 6.36 5 -0.25 (4) +0.04 (5) -0.29 (4) +0.67 (4) +14 +08 -03 -02 -01 +01 20 Ca π 1517 6.36 5 -0.25 (4) +0.04 (5) -0.29 (4) +0.67 (4) +14 +08 -03 -02 -01 +01 20 Ca π 1517 6.36 5 -0.25 (4) +0.04 (5) -0.29 (4) +0.67 (4) +14 +08 -03 -02 -01 +01 20 Ca π 1517 6.36 5 -0.25 (4) +0.04 (5) -0.29 (4) +0.67 (4) +14 +08 -03 -02 -01 +01 20 Ca π 1517 6.36 5 -0.25 (4) +0.04 (5) -0.29 (4) +0.67 (4) +14 +08 -03 -02 -01 +01 20 Ca π 1517 6.36 5 -0.25 (4) +0.04 (5) -0.29 (4) +0.67 (4) +14 +08 -03 -02 -01 +01 20 Ca π 1517 6.36 5 -0.25 (4) +0.04 (5) -0.29 (4) +0.67 (4) +14 +08 -03 -02 -01 +01 20 Ca π 1517 6.36 5 -0.25 (4) +0.04 (5) -0.29 (4) +0.67 (4) +14 +08 -03 -02 -01 +01 20 Ca π 1517 6.36 5 -0.25 (4) +0.04 (5) -0.29 (4) +0.67 (4) +14 +08 -03 -02 -01 +01 20 Ca π 1517 6.36 5 -0.25 (4) +0.01 (5) +0.21 (6) -1.83 (5) +10 +06 -00 -08 +03 +04 20 Ca π 1517 6.36 5 -0.25 (4) +0.01 (4) +0.00 (4) -0.01 (4) +16 +10 -00 -01 -01 +01 20 Ca π 1517 6.36 5 -0.25 (4) +0.01 (4) +0.00 (4) -0.01 (4) +16 +10 -00 -01 -01 +01 20 Ca π 1517 6.36 5 -0.25 (4) +0.01 (5) +0.25 (5) +0.85 (6								, ,			
13		_						, ,			
13 Al π 1653 6.47 1 +0.45 (1) +0.33 (1) +0.12 (1) -05-10 -01-00 +02+03 14 Si π 1310 7.55 49 +0.13 (47) -0.04 (48) +0.20 (47) +11 +06 -00-01 -01+01 14 Si π 1310 7.55 5 +0.17 (4) -0.09 (5) +0.25 (4) -04-09 -03-03 +02+04 16 S π 664 7.21 13 +0.24 (11) +0.12 (11) +0.16 (12) +09+02 -01-01 +00+02 19 K π 1006 5.12 1 -0.08 (1) -0.33 (1) +0.24 (1) +13+09 -01-02 -01+00 20 Ca π 1517 6.36 26 -0.42 (24) +0.01 (21) -0.41 (21) +15+08 -01-05 -01+01 20 Ca π 1517 6.36 5 -0.25 (4) +0.04 (5) -0.29 (4) +02-03 -04-05 +02+02 30 Zn π 726 4.60 4 +0.77 (4) +0.10 (4) +0.67 (4) +14+08 -03-02 -01+01 22 Ti π 1582 4.99 4 -0.01 (4) +0.00 (4) -0.01 (4) +16+10 -00-01 -01+01 22 Ti π 1582 4.99 4 -0.01 (4) +0.00 (4) -0.01 (4) +16+10 -00-01 -01+01 23 Vπ 1429 4.00 1 +0.07 (1) -0.22 (1) +0.29 (1) +18+13 -00-00 -01+01 23 Vπ 1429 4.00 6 +0.32 (6) +0.01 (5) +0.28 (5) +08+05 -02-02 +03+04 24 Cr π 1296 5.67 21 +0.23 (19) -0.08 (19) +0.31 (19) +15+10 -01-02 -01+01 24 Cr π 1296 5.67 32 +0.43 (24) +0.05 (29) +0.40 (24) +0.5+01 -03-03 +03+04 25 Mn π 1158 5.39 11 +0.26 (9) -0.08 (7) +0.36 (9) +15+09 -01-02 -01+01 26 Fe π 1134 7.50 424 +0.34 (424) +0.01 (424) +0.33 (420) +14+09 -02-02 -01+01 26 Fe π 1134 7.50 424 +0.34 (424) +0.01 (5) +0.42 (5) +0.42 (5) +16+12 -02-02 -01 +01 26 Cu π 1037 4.21 1 +0.71 (1) +0.07 (1) +0.65 (1) +17+12 -01-01 -01-01											
$\begin{array}{c ccccccccccccccccccccccccccccccccccc$								` '			
14 Si II 1310 7.55 5 +0.17 (4) -0.09 (5) +0.25 (4) -04 -09 -03 -03 +02 +04 16 S I 664 7.21 13 +0.24 (11) +0.12 (11) +0.16 (12) +09 +02 -01 -01 +00 +02 19 K I 1006 5.12 1 -0.08 (1) -0.33 (1) +0.24 (1) +13 +09 -01 -02 -01 +00 20 Ca I 1517 6.36 26 -0.42 (24) +0.01 (21) -0.41 (21) +15 +08 -01 -05 -01 +01 20 Ca II 1517 6.36 5 -0.25 (4) +0.04 (5) -0.29 (4) +0.2 -03 -04 -05 +02 +02 30 Zn I 726 4.60 4 +0.77 (4) +0.10 (4) +0.67 (4) +14 +08 -03 -02 -01 +01 10 10 10 10 10 10 10 10 10 10 10 10 1						, ,		, ,			
16 S I 664 7.21 13 +0.24 (11) +0.12 (11) +0.16 (12) +09 +02 -01 -01 +00 +02 19 K I 1006 5.12 1 -0.08 (1) -0.33 (1) +0.24 (1) +13 +09 -01 -02 -01 +00 20 Ca I 1517 6.36 26 -0.42 (24) +0.01 (21) -0.41 (21) +15 +08 -01 -05 -01 +01 20 Ca II 1517 6.36 5 -0.25 (4) +0.04 (5) -0.29 (4) +0.2 -03 -04 -05 +02 +02 30 Zn I 726 4.60 4 +0.77 (4) +0.10 (4) +0.67 (4) +14 +08 -03 -02 -01 +01 (LTE analysis)  21 Sc II 1659 3.10 7 -1.57 (6) +0.21 (6) -1.83 (5) +10 +06 -00 -08 +03 +04 22 Ti I 1582 4.99 4 -0.01 (4) +0.00 (4) -0.01 (4) +16 +10 -00 -01 -01 +01 22 Ti II 1582 4.99 60 -0.04 (38) +0.04 (41) -0.07 (38) +09 +05 -02 -03 +03 +04 23 V I 1429 4.00 1 +0.07 (1) -0.22 (1) +0.29 (1) +18 +13 -00 -00 -01 +01 23 V II 1429 4.00 6 +0.32 (6) +0.01 (5) +0.28 (5) +0.8 +05 -02 -02 +03 +04 24 Cr I 1296 5.67 21 +0.23 (19) -0.08 (19) +0.31 (19) +15 +10 -01 -02 -01 +01 24 Cr II 1296 5.67 32 +0.43 (24) +0.05 (29) +0.40 (24) +0.5 +01 -03 -03 +03 +04 25 Mn I 1158 5.39 11 +0.26 (9) -0.08 (7) +0.36 (9) +15 +09 -01 -02 -01 +01 25 Mn II 1158 5.39 1 +0.31 (1) -0.08 (1) +0.39 (1) +0.6 +02 -01 -00 +02 +04 26 Fe II 1134 7.50 424 +0.34 (424) +0.01 (424) +0.33 (420) +14 +09 -02 -02 -01 +01 26 Fe II 1134 7.50 56 +0.40 (56) -0.03 (55) +0.42 (52) +0.5 +01 -03 -01 +03 +04 27 Co I 1352 4.92 5 +0.50 (5) +0.05 (79) +0.06 (74) +14 +09 -01 -01 -01 -01 +01 28 Ni I 1353 6.25 80 +0.63 (77) +0.05 (79) +0.60 (74) +14 +09 -01 -01 -01 -01 +01 29 Cu I 1037 4.21 1 +0.71 (1) +0.07 (1) +0.65 (1) +17 +12 -01 -01 -01 -01 +01 29 Cu I 1037 4.21 1 +0.71 (1) +0.07 (1) +0.65 (1) +17 +12 -01 -01 -01 -01 +01 401 29 Cu I 1037 4.21 1 +0.71 (1) +0.07 (1) +0.65 (1) +17 +12 -01 -01 -01 -01 -01 +01 29 Cu I 1037 4.21 1 +0.71 (1) +0.07 (1) +0.65 (1) +17 +12 -01 -01 -01 -01 -01 +01 29 Cu I 1037 4.21 1 +0.71 (1) +0.07 (1) +0.65 (1) +17 +12 -01 -01 -01 -01 -01 +01 29 Cu I 1037 4.21 1 +0.71 (1) +0.07 (1) +0.65 (1) +17 +12 -01 -01 -01 -01 -01 +01 29 Cu I 1037 4.21 1 +0.71 (1) +0.07 (1) +0.65 (1) +17 +12 -01 -01 -01 -01 -01 +01 29 Cu I 1037 4.21 1 +0.71 (1) +0.07 (1) +0.65 (1) +17 +12 -01 -01 -01 -01											
19 K I 1006 5.12 1 -0.08 (1) -0.33 (1) +0.24 (1) +13 +09 -01 -02 -01 +00 20 Ca I 1517 6.36 26 -0.42 (24) +0.01 (21) -0.41 (21) +15 +08 -01 -05 -01 +01 20 Ca II 1517 6.36 5 -0.25 (4) +0.04 (5) -0.29 (4) +0.2 -03 -04 -05 +02 +02 30 Zn I 726 4.60 4 +0.77 (4) +0.10 (4) +0.67 (4) +14 +08 -03 -02 -01 +01      CLTE analysis    21 Sc II 1659 3.10 7 -1.57 (6) +0.21 (6) -1.83 (5) +10 +06 -00 -08 +03 +04 22 Ti I 1582 4.99 4 -0.01 (4) +0.00 (4) -0.01 (4) +16 +10 -00 -01 -01 +01 22 Ti II 1582 4.99 60 -0.04 (38) +0.04 (41) -0.07 (38) +09 +05 -02 -03 +03 +04 23 V I 1429 4.00 1 +0.07 (1) -0.22 (1) +0.29 (1) +18 +13 -00 -00 -01 +01 23 V II 1429 4.00 6 +0.32 (6) +0.01 (5) +0.28 (5) +0.8 +05 -02 -02 +03 +04 24 Cr II 1296 5.67 21 +0.23 (19) -0.08 (19) +0.31 (19) +15 +10 -01 -02 -01 +01 24 Cr II 1296 5.67 32 +0.43 (24) +0.05 (29) +0.40 (24) +0.5 +01 -03 -03 +03 +04 25 Mn II 1158 5.39 11 +0.26 (9) -0.08 (7) +0.40 (24) +0.5 +01 -03 -03 +03 +04 26 Fe II 1134 7.50 424 +0.34 (424) +0.01 (424) +0.33 (420) +14 +09 -01 -02 -01 +01 26 Fe II 1134 7.50 56 +0.40 (56) -0.03 (55) +0.42 (52) +0.5 +01 -0.3 -01 +03 +04 27 Co I 1352 4.92 5 +0.50 (5) +0.05 (5) +0.05 (5) +0.45 (5) +16 +12 -02 -02 -01 +01 28 Ni I 1353 6.25 80 +0.63 (77) +0.05 (79) +0.60 (74) +14 +09 -01 -01 -01 -01 +01 29 Cu I 1037 4.21 1 +0.71 (1) +0.07 (1) +0.65 (1) +17 +12 -01 -01 -01 -01 +01 29 Cu I 1037 4.21 1 +0.71 (1) +0.07 (1) +0.65 (1) +17 +12 -01 -01 -01 -01 +01 29 Cu I 1037 4.21 1 +0.71 (1) +0.07 (1) +0.65 (1) +17 +12 -01 -01 -01 -01 +01 29 Cu I 1037 4.21 1 +0.71 (1) +0.07 (1) +0.65 (1) +17 +12 -01 -01 -01 -01 +01 29 Cu I 1037 4.21 1 +0.71 (1) +0.07 (1) +0.65 (1) +17 +12 -01 -01 -01 -01 +01 29 Cu I 1037 4.21 1 +0.71 (1) +0.07 (1) +0.65 (1) +17 +12 -01 -01 -01 -01 -01 +01 29 Cu I 1037 4.21 1 +0.71 (1) +0.07 (1) +0.65 (1) +17 +12 -01 -01 -01 -01 -01 +01 29 Cu I 1037 4.21 1 +0.71 (1) +0.07 (1) +0.65 (1) +17 +12 -01 -01 -01 -01 -01 -01 +01 29 Cu I 1037 4.21 1 +0.71 (1) +0.07 (1) +0.65 (1) +17 +12 -01 -01 -01 -01 -01 -01 +01 29 Cu I 1037 4.21 1 +0.71 (1) +0.07 (1) +0.65 (1) +17											
20         Ca I         1517         6.36         26         -0.42 (24)         +0.01 (21)         -0.41 (21)         +15 +08         -01 -05         -01 +01           20         Ca II         1517         6.36         5         -0.25 (4)         +0.04 (5)         -0.29 (4)         +02 -03         -04 -05         +02 +02           30         Zn I         726         4.60         4         +0.77 (4)         +0.10 (4)         +0.67 (4)         +14 +08         -03 -02         -01 +01           (LTE analysis)           21         Sc II         1659         3.10         7         -1.57 (6)         +0.21 (6)         -1.83 (5)         +10 +06         -00 -08         +03 +04           22         Ti I         1582         4.99         4         -0.01 (4)         +0.00 (4)         -0.01 (4)         +16 +10         -00 -01         -01 +01           22         Ti II         1582         4.99         60         -0.04 (38)         +0.04 (41)         -0.07 (38)         +09 +05         -02 -03         +03 +04           23         V II         1429         4.00         1         +0.07 (1)         -0.22 (1)         +0.29 (1)         +18 +13         -00 -00         -01 +01								, ,			
20         Ca II         1517         6.36         5         -0.25 (4)         +0.04 (5)         -0.29 (4)         +02 -03         -04 -05         +02 +02           30         Zn I         726         4.60         4         +0.77 (4)         +0.10 (4)         +0.67 (4)         +14 +08         -03 -02         -01 +01           (LTE analysis)           21         Sc II         1659         3.10         7         -1.57 (6)         +0.21 (6)         -1.83 (5)         +10 +06         -00 -08         +03 +04           22         Ti I         1582         4.99         4         -0.01 (4)         +0.00 (4)         -0.01 (4)         +16 +10         -00 -01         -01 +01           22         Ti II         1582         4.99         60         -0.04 (38)         +0.04 (41)         -0.07 (38)         +09 +05         -02 -03         +03 +04           23         V I         1429         4.00         1         +0.07 (1)         -0.22 (1)         +0.29 (1)         +18 +13         -00 -00         -01 +01           23         V II         1429         4.00         6         +0.32 (6)         +0.01 (5)         +0.28 (5)         +08 +05         -02 -02         +03 +04											
Carr   726   4.60   4   +0.77   (4)   +0.10   (4)   +0.67   (4)   +14 +08   -03 -02   -01 +01						, ,					
CLTE analysis   CLTE analysi						, ,	, ,	` '			
21 Sc II 1659 3.10 7 -1.57 (6) +0.21 (6) -1.83 (5) +10+06 -00-08 +03+04 22 Ti I 1582 4.99 4 -0.01 (4) +0.00 (4) -0.01 (4) +16+10 -00-01 -01+01 22 Ti II 1582 4.99 60 -0.04 (38) +0.04 (41) -0.07 (38) +09+05 -02-03 +03+04 23 V I 1429 4.00 1 +0.07 (1) -0.22 (1) +0.29 (1) +18+13 -00-00 -01+01 23 V II 1429 4.00 6 +0.32 (6) +0.01 (5) +0.28 (5) +08+05 -02-02 +03+04 24 Cr I 1296 5.67 21 +0.23 (19) -0.08 (19) +0.31 (19) +15+10 -01-02 -01+01 24 Cr II 1296 5.67 32 +0.43 (24) +0.05 (29) +0.40 (24) +05+01 -03-03 +03+04 25 Mn I 1158 5.39 11 +0.26 (9) -0.08 (7) +0.36 (9) +15+09 -01-02 -01+01 25 Mn II 1158 5.39 1 +0.31 (1) -0.08 (1) +0.39 (1) +06+02 -01-00 +02+04 26 Fe II 1134 7.50 424 +0.34 (424) +0.01 (424) +0.33 (420) +14+09 -02-02 -01+01 26 Fe II 1134 7.50 56 +0.40 (56) -0.03 (55) +0.42 (52) +05+01 -03-01 +03+04 27 Co I 1352 4.92 5 +0.50 (5) +0.05 (5) +0.45 (5) +16+12 -02-02 -01+01 28 Ni I 1353 6.25 80 +0.63 (77) +0.05 (79) +0.60 (74) +14+09 -01-01 -01 +01 29 Cu I 1037 4.21 1 +0.71 (1) +0.07 (1) +0.65 (1) +17+12 -01-01 -01 +01		2111	720	7.00		10.77 (4)	, ,	10.07 (4)	114 100	03 02	01 101
22 Ti I 1582 4.99 4 -0.01 (4) +0.00 (4) -0.01 (4) +16+10 -00-01 -01+01 22 Ti II 1582 4.99 60 -0.04 (38) +0.04 (41) -0.07 (38) +09+05 -02-03 +03+04 23 V I 1429 4.00 1 +0.07 (1) -0.22 (1) +0.29 (1) +18+13 -00-00 -01+01 23 V II 1429 4.00 6 +0.32 (6) +0.01 (5) +0.28 (5) +08+05 -02-02 +03+04 24 Cr I 1296 5.67 21 +0.23 (19) -0.08 (19) +0.31 (19) +15+10 -01-02 -01+01 24 Cr II 1296 5.67 32 +0.43 (24) +0.05 (29) +0.40 (24) +05+01 -03-03 +03+04 25 Mn I 1158 5.39 11 +0.26 (9) -0.08 (7) +0.36 (9) +15+09 -01-02 -01+01 25 Mn II 1158 5.39 1 +0.31 (1) -0.08 (1) +0.39 (1) +06+02 -01-00 +02+04 26 Fe I 1134 7.50 424 +0.34 (424) +0.01 (424) +0.33 (420) +14+09 -02-02 -01+01 26 Fe II 1134 7.50 56 +0.40 (56) -0.03 (55) +0.42 (52) +05+01 -03-01 +03+04 27 Co I 1352 4.92 5 +0.50 (5) +0.05 (5) +0.45 (5) +16+12 -02-02 -01+01 28 Ni I 1353 6.25 80 +0.63 (77) +0.05 (79) +0.60 (74) +14+09 -01-01 -01 +01 29 Cu I 1037 4.21 1 +0.71 (1) +0.07 (1) +0.65 (1) +17+12 -01-01 -01+01	21	Sc II	1659	3 10	7	-1.57 (6)		-1.83 (5)	+10 +06	-00 -08	+03 +04
22 Ti π 1582 4.99 60  -0.04 (38) +0.04 (41)  -0.07 (38) +09 +05  -02 -03 +03 +04   23 V π 1429 4.00 1 +0.07 (1) -0.22 (1) +0.29 (1) +18 +13 -00 -00 -01 +01   23 V π 1429 4.00 6 +0.32 (6) +0.01 (5) +0.28 (5) +08 +05 -02 -02 +03 +04   24 Cr π 1296 5.67 21 +0.23 (19) -0.08 (19) +0.31 (19) +15 +10 -01 -02 -01 +01   24 Cr π 1296 5.67 32 +0.43 (24) +0.05 (29) +0.40 (24) +0.5 +01 -03 -03 +03 +04   25 Mn π 1158 5.39 11 +0.26 (9) -0.08 (7) +0.36 (9) +15 +09 -01 -02 -01 +01   25 Mn π 1158 5.39 1 +0.31 (1) -0.08 (1) +0.39 (1) +0.6 +02 -01 -00 +02 +04   26 Fe π 1134 7.50 424 +0.34 (424) +0.01 (424) +0.33 (420) +14 +09 -02 -02 -01 +01   26 Fe π 1134 7.50 56 +0.40 (56) -0.03 (55) +0.42 (52) +0.5 +01 -03 -01 +03 +04   27 Co π 1352 4.92 5 +0.50 (5) +0.05 (5) +0.45 (5) +16 +12 -02 -02 -01 +01   28 Ni π 1353 6.25 80 +0.63 (77) +0.05 (79) +0.60 (74) +14 +09 -01 -01 -01 -01 +01   29 Cu π 1037 4.21 1 +0.71 (1) +0.07 (1) +0.65 (1) +17 +12 -01 -01 -01 -01 +01							, ,				
23 V I 1429 4.00 1 +0.07 (1) -0.22 (1) +0.29 (1) +18 +13 -00 -00 -01 +01 23 V II 1429 4.00 6 +0.32 (6) +0.01 (5) +0.28 (5) +08 +05 -02 -02 +03 +04 24 Cr I 1296 5.67 21 +0.23 (19) -0.08 (19) +0.31 (19) +15 +10 -01 -02 -01 +01 24 Cr II 1296 5.67 32 +0.43 (24) +0.05 (29) +0.40 (24) +0.5 +01 -0.3 -0.3 +0.3 +0.4 25 Mn II 1158 5.39 11 +0.26 (9) -0.08 (7) +0.36 (9) +15 +09 -01 -02 -01 +01 25 Mn II 1158 5.39 1 +0.31 (1) -0.08 (1) +0.39 (1) +0.6 +02 -01 -00 +02 +0.4 26 Fe I 1134 7.50 424 +0.34 (424) +0.01 (424) +0.33 (420) +14 +09 -02 -02 -01 +01 26 Fe II 1134 7.50 56 +0.40 (56) -0.03 (55) +0.42 (52) +0.5 +01 -0.3 -01 +0.3 +0.4 27 Co I 1352 4.92 5 +0.50 (5) +0.05 (5) +0.05 (5) +0.45 (5) +16 +12 -02 -02 -01 +01 28 Ni I 1353 6.25 80 +0.63 (77) +0.05 (79) +0.60 (74) +14 +09 -01 -01 -01 -01 +01 29 Cu I 1037 4.21 1 +0.71 (1) +0.07 (1) +0.65 (1) +17 +12 -01 -01 -01 -01 +01							, ,	, ,			
23 V II 1429 4.00 6 +0.32 (6) +0.01 (5) +0.28 (5) +08 +05 -02 -02 +03 +04 24 Cr I 1296 5.67 21 +0.23 (19) -0.08 (19) +0.31 (19) +15 +10 -01 -02 -01 +01 24 Cr II 1296 5.67 32 +0.43 (24) +0.05 (29) +0.40 (24) +0.5 +01 -0.3 -0.3 +0.3 +0.4 25 Mn I 1158 5.39 11 +0.26 (9) -0.08 (7) +0.36 (9) +15 +09 -01 -02 -01 +01 25 Mn II 1158 5.39 1 +0.31 (1) -0.08 (1) +0.39 (1) +0.6 +0.2 -01 -0.0 +0.2 +0.4 26 Fe I 1134 7.50 424 +0.34 (424) +0.01 (424) +0.33 (420) +14 +0.9 -0.2 -0.2 -0.1 +0.1 26 Fe II 1134 7.50 56 +0.40 (56) -0.03 (55) +0.42 (52) +0.5 +0.1 -0.3 -0.1 +0.3 +0.4 27 Co I 1352 4.92 5 +0.50 (5) +0.05 (5) +0.05 (5) +0.45 (5) +1.6 +12 -0.2 -0.2 -0.1 +0.1 28 Ni I 1353 6.25 80 +0.63 (77) +0.05 (79) +0.60 (74) +14 +09 -0.1 -0.1 -0.1 +0.1 29 Cu I 1037 4.21 1 +0.71 (1) +0.07 (1) +0.65 (1) +1.7 +1.2 -0.1 -0.1 -0.1 +0.1						, ,		, ,			
24											
24											
25 Mn I 1158 5.39 11 +0.26 (9) -0.08 (7) +0.36 (9) +15 +09 -01 -02 -01 +01 25 Mn II 1158 5.39 1 +0.31 (1) -0.08 (1) +0.39 (1) +06 +02 -01 -00 +02 +04 26 Fe I 1134 7.50 424 +0.34 (424) +0.01 (424) +0.33 (420) +14 +09 -02 -02 -01 +01 26 Fe II 1134 7.50 56 +0.40 (56) -0.03 (55) +0.42 (52) +05 +01 -03 -01 +03 +04 27 Co I 1352 4.92 5 +0.50 (5) +0.05 (5) +0.45 (5) +16 +12 -02 -02 -01 +01 28 Ni I 1353 6.25 80 +0.63 (77) +0.05 (79) +0.60 (74) +14 +09 -01 -01 -01 +01 29 Cu I 1037 4.21 1 +0.71 (1) +0.07 (1) +0.65 (1) +17 +12 -01 -01 -01 +01						, ,		, ,			
25 Mn II 1158 5.39 1 +0.31 (1) -0.08 (1) +0.39 (1) +06 +02 -01 -00 +02 +04 26 Fe I 1134 7.50 424 +0.34 (424) +0.01 (424) +0.33 (420) +14 +09 -02 -02 -01 +01 26 Fe II 1134 7.50 56 +0.40 (56) -0.03 (55) +0.42 (52) +05 +01 -03 -01 +03 +04 27 Co I 1352 4.92 5 +0.50 (5) +0.05 (5) +0.45 (5) +16 +12 -02 -02 -01 +01 28 Ni I 1353 6.25 80 +0.63 (77) +0.05 (79) +0.60 (74) +14 +09 -01 -01 -01 +01 29 Cu I 1037 4.21 1 +0.71 (1) +0.07 (1) +0.65 (1) +17 +12 -01 -01 -01 +01						, ,	, ,				
26 Fe I 1134 7.50 424 +0.34 (424) +0.01 (424) +0.33 (420) +14 +09 -02 -02 -01 +01 26 Fe II 1134 7.50 56 +0.40 (56) -0.03 (55) +0.42 (52) +05 +01 -03 -01 +03 +04 27 Co I 1352 4.92 5 +0.50 (5) +0.05 (5) +0.45 (5) +16 +12 -02 -02 -01 +01 28 Ni I 1353 6.25 80 +0.63 (77) +0.05 (79) +0.60 (74) +14 +09 -01 -01 -01 +01 29 Cu I 1037 4.21 1 +0.71 (1) +0.07 (1) +0.65 (1) +17 +12 -01 -01 -01 +01								` '			
26 Fe II 1134 7.50 56 +0.40 (56) -0.03 (55) +0.42 (52) +05 +01 -03 -01 +03 +04 27 Co I 1352 4.92 5 +0.50 (5) +0.05 (5) +0.45 (5) +16 +12 -02 -02 -01 +01 28 Ni I 1353 6.25 80 +0.63 (77) +0.05 (79) +0.60 (74) +14 +09 -01 -01 -01 +01 29 Cu I 1037 4.21 1 +0.71 (1) +0.07 (1) +0.65 (1) +17 +12 -01 -01 -01 +01							, ,				
27 Co I 1352 4.92 5 +0.50 (5) +0.05 (5) +0.45 (5) +16+12 -02-02 -01+01 28 Ni I 1353 6.25 80 +0.63 (77) +0.05 (79) +0.60 (74) +14+09 -01-01 -01+01 29 Cu I 1037 4.21 1 +0.71 (1) +0.07 (1) +0.65 (1) +17+12 -01-01 -01+01				7.50	56	` '		, ,			
28 Ni I 1353 6.25 80 +0.63 (77) +0.05 (79) +0.60 (74) +14 +09 -01 -01 -01 +01 29 Cu I 1037 4.21 1 +0.71 (1) +0.07 (1) +0.65 (1) +17 +12 -01 -01 -01 +01		Со і		4.92				, ,			-01 + 01
	28	Ni 1	1353	6.25	80				+14 +09	-01 -01	-01 + 01
	29	Cu 1	1037	4.21	1	+0.71 (1)	+0.07 (1)	+0.65 (1)	+17 +12	-01 -01	-01 + 01
34 SCI U9/ 3.33 I +U.31 (1) +U.2/ (1) +U.24 (1) +12 +U3 -U0 -U0 +U2	34	Se 1	697	3.35	1	+0.51 (1)	+0.27 (1)	+0.24 (1)	+12 +05	-00 -00	-00 + 02
38 Sr II 1464 2.90 4 +0.99 (1) +0.37 (2) +0.52 (1) +11 +04 -05 -04 +02 +04	38	Sr 11	1464	2.90	4	+0.99 (1)	+0.37 (2)		+11 +04	-05 -04	+02 +04
39 Y II 1659 2.24 12 +1.28 (7) +0.45 (11) +0.84 (7) +11 +07 -03 -03 +02 +04	39	Yп	1659	2.24	12	+1.28 (7)			+11 +07	-03 - 03	+02 +04
40 Zr II 1741 2.60 8 +1.19 (5) +0.54 (6) +0.73 (6) +09 +06 -02 -01 +03 +04											
56 Ba II 1455 2.13 4 +1.51 (1) +0.54 (3) +1.20 (1) +19+12 -11-11 +01+03		Вап		2.13						-11 -11	+01 +03
57 La II 1578 1.22 5 +1.25 (3) +0.46 (5) +0.77 (3) +16+10 -02-02 +02+04									+16 +10	-02 -02	
58 Ce II 1478 1.55 4 +1.30 (4) +0.52 (4) +0.78 (4) +13 +09 -01 -00 +02 +04	58	Се п	1478	1.55	4	+1.30 (4)	+0.52 (4)		+13 +09	-01 -00	+02 +04
60 Nd II 1602 1.50 2 +1.10 (2) +0.22 (2) +0.88 (2) +17 +11 -01 -00 +01 +03	60	Nd 11	1602	1.50	2	+1.10 (2)	+0.22 (2)		+17 +11	-01 -00	+01 +03
63 Eu п 1356 0.51 2 +1.28 (1) +0.40 (2) +1.07 (1) +15 +10 -04 -01 +02 +04	63	Еи п	1356	0.51	2	+1.28 (1)	+0.40 (2)	+1.07 (1)	+15 +10	-04 -01	+02 +04

(1) Atomic number. (2) Element species. (3) 50% condensation temperature (in K) taken from Table 8 of Lodders (2003). (4) Reference solar abundances (in the usual normalization of H = 12.00) taken from Anders & Grevesse's (1989) compilation, except that 7.50 is adopted for Fe and the solar system abundance of 3.28 (Lodders 2003) is used for Li corresponding to the young Sun. (5) Number of lines adopted for this species. (6) Mean of [X/H]<sub>A</sub> (relative abundance for A in comparison with the Sun) averaged over lines. (7) Actual number of lines used for deriving  $\langle [X/H]_A \rangle$ . (8) Mean of [X/H]<sub>B</sub>. (9) Actual number of lines employed for  $\langle [X/H]_B \rangle$ . (10) Mean of  $\Delta A_{A-B}^X$  (line-by-line differential abundance between A and B) averaged over lines. (11) Actual number of lines used for calculating  $\langle \Delta A_{A-B}^X \rangle$ . (12) Abundance change for A in response to  $\Delta T_{\rm eff} = +300$  K. (13) Abundance change for B in response to  $\Delta V_{\rm eff} = +300$  K. (14) Abundance change for A in response to  $\Delta V_{\rm t} = +0.3$  km s<sup>-1</sup>. (15) Abundance change for B in response to  $\Delta V_{\rm t} = +0.3$  km s<sup>-1</sup>. (16) Abundance change for A in response to  $\Delta I_{\rm t} = +0.3$  km s<sup>-1</sup>. (17) Abundance change for B in response to  $\Delta I_{\rm t} = +0.3$  km s<sup>-1</sup>. (18) Abundance change for B in response to  $\Delta I_{\rm t} = +0.3$  km s<sup>-1</sup>. (19) Abundance change for B in response to  $\Delta I_{\rm t} = +0.3$  km s<sup>-1</sup>. (19) Abundance change for B in response to  $\Delta I_{\rm t} = +0.3$  km s<sup>-1</sup>. (19) Abundance change for B in response to  $\Delta I_{\rm t} = +0.3$  km s<sup>-1</sup>. (19) Abundance change for B in response to  $\Delta I_{\rm t} = +0.3$  km s<sup>-1</sup>. (19) Abundance change for B in response to  $\Delta I_{\rm t} = +0.3$  km s<sup>-1</sup>. (19) Abundance change for B in response to  $\Delta I_{\rm t} = +0.3$  km s<sup>-1</sup>. (19) Abundance change for B in response to  $\Delta I_{\rm t} = +0.3$  km s<sup>-1</sup>. (19) Abundance change for B in response to  $\Delta I_{\rm t} = +0.3$  km s<sup>-1</sup>. (19) Abundance change for B in response to  $\Delta I_{\rm t} = +0.3$  km s<sup>-1</sup>. (19) Abundance change for B in response to  $\Delta I_{\rm t} = +0.3$  km s<sup>-1</sup>. (19)